Reexamination of the Pyrolysis of Polyethylene: Data Needs, Free-Radical Mechanistic Considerations, and Thermochemical Kinetic Simulation of Initial Product-Forming Pathways

Marvin L. Poutsma†

Chemical Sciences Division, Oak Ridge National Laboratory, P.O. Box 2008, Oak Ridge, Tennessee 37831-6197

Received July 9, 2003; Revised Manuscript Received September 22, 2003

ABSTRACT: Gaps in the voluminous data on pyrolysis of polyethylene that impede mechanistic understanding are highlighted, especially for H:C material balances, product distributions at varying conversions in isothermal closed systems, and inconsistencies between GC and FIMS analyses of products with lower volatility. Thermochemical kinetic estimates are made for the rates of various initiation processes; these suggest that molecular disproportionation contributes to chain initiation, along with homolysis, at lower M_n. Simulations indicate that the standard statistical test for random scission, a linear relationship between log N_c and c for volatile products, is not generally valid in *open* systems, and its empirical observation implies restrictions on the dependence of the rate of volatilization on c. Simulations of the *initial* distributions of volatile products and residue functionalities were performed based on propagation rate constants estimated by thermochemical kinetic procedures. The practice of deducing the amount of backbiting from positive deviations at lower c from the linear log N_c−c relationship established for higher c values is shown to underestimate the fraction of backbiting because the latter will give some products at *every* c so long as the 1,5-shift is not exclusive ($k_{15} \gg k_{16} > k_{14}$). Compositions of volatiles at finite conversions were simulated by formal superposition of (a) backbiting and unzipping products predicted from this kinetic model and (b) random scission products, which form only after multiple bond cleavages, predicted from a statistical model. Comparisons with experimental data showed some success but were limited by data gaps and inconsistencies.

Introduction

Thermal decomposition[1] of vinyl polymers, $(CH_2CRX)_n$ with R = H or alkyl and X = H, alkyl, aryl, halogen, CO_2R', CN, etc., is relevant to deterioration of materials properties during high-temperature processing and use, pyrolysis-based analytical methods,[1h] and potential pyrolytic methods to recover chemical feedstock or fuel values from polymer waste. Recent research has emphasized reactor and process design to maximize product value, extraction of kinetic models from thermogravimetric analysis (TGA) data, and evolution of the changes in molecular weight (MW) of the degrading residue. Much less attention has been given to mechanistic modeling, particularly of the composition of the volatiles, at the molecular level. Our purpose is to examine existing mechanistic conclusions in light of known free-radical chemistry, to critique existing models, to explore the application of the thermochemical kinetic approach to elementary reaction steps, and, in the process, to identify critical data gaps. We begin with the simplest prototype polyethylene (PE).[1i]

Three classes of bond cleavage are recognized, regardless of mechanism. (1) Breaking a backbone C−C bond and formal 1,3-hydrogen shift leads to new saturated and unsaturated end groups. If such random scission (RS) events are repeated successively in a polymer and its degrading products, the result is initially a decrease in MW and ultimately weight loss as degraded products, with a broad range of carbon numbers (c), become small enough to evaporate without further cleavage. (2) Volatile products may be clipped from the end of a polymer chain from the very beginning of reaction, with a c distribution that is not random, by a process of end scission or backbiting (BB). (3) Finally, the monomer may be regenerated by a process of unzipping (UZ). In addition to these cleavages, enlargement processes can occur at the lowest reaction temperatures (T) that increase MW and may also increase polymer branching.

Data Overview

Methods. Kinetic and product data for pyrolysis of molten PE are voluminous but inconsistent. Differences between high-density PE (HDPE) prepared with metal-containing catalysts and low-density PE (LDPE) prepared with radical initiators and containing more chain branching[2,3] are subtle and not always clear.[4]

Dynamic TGA data, which record the fraction of weight loss (x) as a function of T and time (t), reveal the onset of weight loss for PE at ≥400 °C and its completion by 500 °C with negligible residue remaining. However, decreases in MW occur already at ≤300 °C before significant volatiles form. Laboratory-scale isothermal studies in the "low-T regime" (≤500 °C) are typically performed in the TGA mode or in open reactors from which volatiles are continuously removed by an inert sweep gas or under vacuum over periods of minutes−hours for later off-line analysis. There is negligible data from small closed reactors without significant headspace such that all products are forced to remain in the reacting polymer melt. In the "high-T regime" (≥500 °C), very high nominal heat-up rates are typically used to achieve $x = 1$ as rapidly as possible ("flash pyrolyses") and allow direct interfacing with analytical apparatus. Configurations feature small samples with resistively heated filaments or ribbons or inductively coupled Curie-point heaters.[6−8] Because of

† Retired Guest Scientist. E-mail poutsmaml@ornl.gov.

10.1021/ma0303768 CCC: $25.00
Published on Web 11/05/2003

heat transfer limitations and the endothermic nature of pyrolysis reactions,[1c,g,9] it appears prudent to consider quoted T's as upper limits.

We will refer less frequently to data from larger samples in pilot-scale apparatus designed for tertiary recycling of polymer waste. Lower-T examples include sealed reactors,[10−12] "reactive distillation" systems,[13−16] fluidized-bed reactors in which molten PE is dispersed on an inert carrier,[17a,18] and continuously stirred tank reactors (CSTR).[19] Higher-T examples, in which a sequential breakdown of polymer to wax to gas oil to naphtha to gas is indicated as conditions become more forcing and degradation occurs in both the melt and the gas phase, include fluidized-bed reactors,[17b,c,20−24] rotating cone pyrolyzers,[25a,b] and tubular reactors with comparatively long residence times.[25c,26] Under extreme conditions, significant yields of ethylene, propylene, and methane as well as aromatics[24c,26b] can be achieved. The ultimate thermodynamic driving force is in fact toward hydrogen-depleted aromatics ("coke") and methane[25c] by secondary reactions that are qualitatively different from the free-radical chain to be discussed below.[27]

Kinetics. Dickens[28] reviewed early TGA studies, Westerhout and co-workers[25d] critically reviewed later data and the difficulties in extracting mechanistically relevant information, and Ceamanos and co-workers[29] provided an even more recent compilation; numerous recent TGA data sets and approaches to their interpretation are available.[18b,30a,31,32,33a,b,34,35] The kinetics of coupled cleavage and evaporation were first formulated by Simha and Wall,[36] who provided analytical solutions for MW changes in the residue, using the simplifying assumption that a first-order evaporation process changes discontinuously from nonexistent to totally dominant when the MW decreases through a critical value L_c.[30a,35a,b,36] There are indications of sample size/surface area/pressure effects[28,37] and a role for bubble formation[30b] which suggest kinetic limitations from evaporation[31a] superimposed on the chemical kinetics.

TGA data treatments commonly assume a "single-step" reaction with a "lumped" rate constant, k, and a power-law kinetic order, n,[38] that is allowed to vary with the progress of the pyrolysis, i.e., $dx/dt = k(1 - x)^n = A \exp(-E/RT)(1 - x)^n$. Derived values of the global A, E, and n parameters vary widely; e.g., Westerhout[25d] reported a range of $E = 38-76$ kcal mol^{-1}. Even though A and E somewhat compensate,[29,34b,35b] 10-fold variations still exist in k and have been ascribed to effects of PE type and MW, the inadequacy of the power-law model,[35b,39] and experimental error. Typically n increases from ≈0 at low x to ≈1 at high x; hence, the common use of $n = 1$ applies only to the regime where most of the initial decomposition is already finished. Hence, the usefulness of TGA parameters for mechanistic analysis is limited. Further ambiguities arise in the dynamic TGA mode where dx/dt increases with increasing T because both rate constants and L_c increase.[35b] More recent approaches to formulate kinetic data, particularly for the evolution of the molecular weight distribution (MWD), have used continuous distribution kinetics and the method of moments to derive kinetic solutions;[40] however, use of a small number of lumped rate constants is still most common.[41]

Initial Changes in the Polymer Residue. Decreases in MW occur before volatilization begins;[42−45,46b,47−51] representative data at 315−390 °C are collected in Table S1 of the Supporting Information. Formal rate constants for the MW decrease, derived for ideal RS,[1a,c,52] are not typically constant but indicate a "fast" followed by a "slow" phase.[42−45,46b,47a,48,53] At ≥400 °C where volatilization commences, the rapid rate of decrease of MW is obscured by the nonzero heat-up time characteristic of batch reactors. In contrast, at lower T (≤300 °C), the MWD develops a shoulder at higher MW, in competition with degradation,[31a,46b] that has been attributed to formation of new LCBs[46b] or "repolymerization".[31a] Several recent examples of LCB formation exist.[47,49,51] In the even lower-T processing range (190−250 °C), there is also evidence for formation of LCBs[54] or "cross-linking".[55]

Oakes and Richards[42] demonstrated increased unsaturation along with decreasing MW at 315−360 °C. The average number of double bonds per molecule, f_t, remained ≈1 as M_n decreased, in conformance with stoichiometric constraints for negligible volatilization. TV groups grew in continuously, but VD and VL groups plateaued for $M_n < 1000$. Others have also reported ingrowth of predominantly TV groups with lesser amounts of the other structures.[46b,47b,50,56] For a Phillips HDPE with initially largely one methyl and one TV end group, f_t fell below 1 for longer reaction times at 350−390 °C,[47] in contrast with data of Oakes and Richards.[42] Such a decrease in f_t from 1.02 to 0.57 has also been reported[49] for Phillips HDPE after 6 h at 370 °C.

Volatile Products. The volatiles are largely linear alkanes (ANE), 1-alkenes (ENE), and, at higher T, α,ω-dienes (DIENE). Much smaller amounts of branched products, more prevalent from LDPE than HDPE, have been used to diagnose the nature of the SCBs in the former.[57,58a,59,60] Despite large amounts of episodic GC and MS data (see Tables S2−S4 of the Supporting Information for key references), quantitative results on N_c (the mole fraction of products with c carbons or the relative mole fractions over a detected c range) and the ANE:ENE:DIENE ratios vs c are less prevalent because of the common absence of calibration factors, condensation/sorption in GC systems that create biases in the upper c range,[9,61] and use of cold-trapping schemes that also create c biases.

Light Gases. Quantitative data for the small fraction of C_{1-5} hydrocarbons produced at lower T are compiled in Table S2 and Figure 1.[7b,20,43,56,62−66] The scatter illustrates the difficulty in separating effects of reaction conditions and PE type from data uncertainties. However, if we exclude pioneering data[43,62] from uncalibrated MS analyses and the atypically high ethylene yield from a flash pyrolysis run at 500 °C[20] (the broken lines in Figure 1), the remaining data from GC analyses for a range of x values (the solid lines), all for HDPE or PM, suggest that propylene and propane are the most prominent. For C_{3-5}, the ANE:ENE ratios are 0.7−0.9 with that for C_2 being higher (≈1.4) and more variable. The very modest selectivity to monomer (the UZ pathway) is clear. Effects of T, and the associated increase in x, appear to be modest.[56,62,63a] From exhaustive Curie-point pyrolysis of HDPE at much higher T (770 °C), Willmott[7a] reported the molar distribution methane:ethane:ethylene:propane:propylene:butane:1-butene:1,3-butadiene = 7:9:30:23:12:8:4:6; for parallel results at 480 °C[7b] the proportion of 1,3-butadiene was much lower (see below). In some studies in the high-T regime, the pattern $C_3 > C_2$ persists (Table S4), but counter-examples also exist, all from flash pyrolyses of LDPE.[20a,b,67b,68,69]

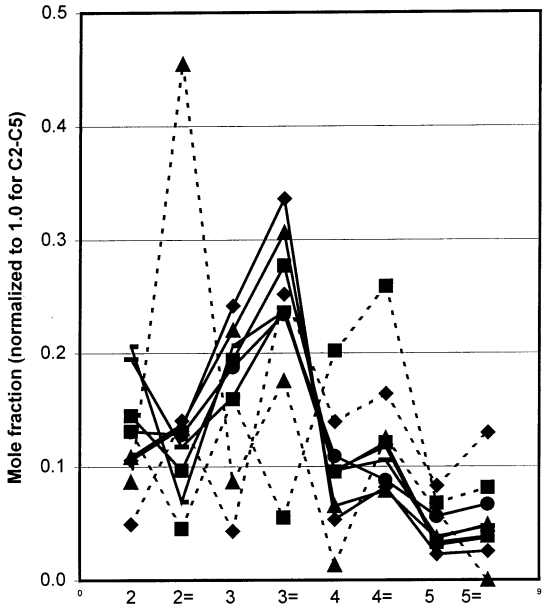

Figure 1. Distributions of individual C_{2-5} hydrocarbons from low-*T* pyrolyses of PE: solid line ■, HDPE, 415 °C, 10 min, GC, ref 56; solid line ♦, HDPE, 375 °C, 20 min, GC, ref 63a; solid line ▲, HDPE, 425 °C, 20 min, GC, ref 63a; solid line ●, PM, 437 °C, 20 min, GC, ref 63b; solid line −, HDPE, 420 °C, 150 min, GC, ref 64; solid line —, HDPE, 420 °C, 15 h, GC, ref 65; broken line ■, PE, 405−475 °C, 30 min, MS, ref 62; broken line ♦, PM, 405−475 °C, 30 min, MS, ref 43; broken line ▲, PE, 500 °C, 20 s, GC, ref 20.

Higher Products at Lower Temperatures. Results at lower *T* with GC analyses for heavier products and resolution often to $c \geq 30$ are compiled in Table S3.[32,33,60,64,66b,70−75] (Recently GC resolution has been achieved to $c = 50^{+}$.[22,61]) We suggest that the most reliable GC approaches minimize preliminary sample fractionation and use FID detection, for which the assumption that signal intensity is proportional to *c*, i.e., wt %, is quite good.[76] In contrast, use of uncalibrated GC/MS responses for mixtures with varying functionality to represent either mol % or wt % is questionable. At low *T*, DIENEs were at best trivial products compared with ANEs and ENEs for the *c* ranges reported, even at high *x*.[32,33,70,72] In a direct comparison at low *x*, HDPE gave a heavier C_{3-13} product than LDPE,[60] and small amounts of branched products, especially at low *x*, were more prevalent from LDPE,[60,73] consistent with its more branched structure. De Witt and Broadbelt[64] provided data for C_{1-5} and C_{8-24} ANEs and ENEs (no DIENEs noted) formed from HDPE at 420 °C as a function of varying *x* ($t = 30-150$ min; $x \approx 0.04-0.35$).[77] A closed system was used with a relatively large headspace volume, and the authors proposed that some "late" degradation occurred in the gas phase, especially for ENE products and for the higher sample loadings which led to higher gas-phase product pressures.

In contrast, the pyrolysis/field-ionization mass spectrometry (FIMS) technique, which features a very short transfer distance in a vacuum from a heated insertion probe to the field emitter and soft ionization of the volatiles with minimal fragmentation, detects much larger products in the earliest stages of decomposition and suggests that GC analyses sample only a lower-*c* portion of the volatiles. Lattimer[78] summed spectra from LDPE and HDPE over a multiminute period at 395−400 °C (presumably low *x*) and detected products in the C_{14-114} range with the dominant homologous series throughout being ENEs with maximum intensity at C_{33} and C_{36}. An ANE series was much less prevalent, and the ANE:ENE ratio appeared to decrease as *c* increased, in opposition to trends in GC data at lower *c* (Table S3). A small DIENE series was also observed, and the DIENE:ENE ratio appeared to increase as *c* increased. Unfortunately no calibration was presented, such that the quantitation of N_c vs *c* and the ANE:ENE:DIENE ratios may be in question.[79] This concern is reinforced by data in the C_{15-30} range where the techniques overlap: FIMS suggested dominant ENEs with essentially no ANEs, in contrast to the extensive GC results (Table S3).[80] An earlier pyrolysis−FIMS study[81] programmed at ≈1 °C/s revealed even larger products up to C_{140}, but no discrimination among ANEs, ENEs, and DIENEs was made; a bimodal distribution with maxima near C_{40} and C_{70} and a minimum near C_{60} was not further discussed. Pyrolysis−GC fractography[82] also recently revealed products from HDPE at 600 °C up to C_{100} but with less than unit *c* resolution on a broad background. On the basis of rates of vaporization and ΔH_v, Wall and co-workers[83] estimated that alkanes up to C_{100} could indeed vaporize from degrading PE without further decomposition at ≈400 °C under high vacuum, in qualitative agreement with the estimate of Simha and Wall[36] that $L_c \approx 72$ under these conditions.

Fluidized-bed pyrolysis at intermediate *T* with high flows of fluidizing gas allows collection overhead of significant amounts of high-MW "waxes". LDPE at 500 °C[22] gave 45 wt % wax for which GC resolution was achieved for the range $c = 14-57$; ENEs dominated both ANEs and DIENEs, in agreement with FIMS results, but no quantitation was given. Similarly, HDPE at 510 °C gave[17a] >60 wt % of waxes with $T_b > 500$ °C, corresponding to C_{36+}.[34b,84] Waxes obtained in 80 wt % yield from LDPE and HDPE at 450 °C in a conical spouted fluidized-bed reactor[18a] had MWs approaching C_{1000}. However, on the basis of estimated T_b values, e.g., 715 °C for C_{100},[84] we question whether such large products in this example truly evaporated at 450 °C or whether aerosol formation from partially degraded PE occurred.

In summary, the combined data suggests that volatiles are formed at every *c* value to an upper limit established by the capability of the analytical technique[9,61,78,81,82] and/or the volatility of hydrocarbons at the *T* and pressure of the pyrolysis.[83] Because no single technique appears to have been able to provide calibrated quantitative N_c distributions over the entire c range, there remains a critical need for such data as a function of conditions.

Higher Products at Higher Temperatures. Results from studies at higher *T*,[6a,b,9,20,22,30b,57,58,61,67,68,74,85−87] typically under flash conditions that achieve $x = 1$ with in-line GC analyses, are compiled in Table S4. The N_c-c distributions and the emergence of DIENEs as more significant products are discussed below. Prompted by a deficiency of H in the volatiles at higher *T*, Wampler[67b] detected formation of H_2, which sharply increased with increasing *T* over the range 600−900 °C but was not quantified; however, less dramatic dependences of small H_2 yields on *T* have also been reported.[24c,40]

The Free-Radical Chain Mechanism. Although backbone scission to form a saturated chain end (PANE) and an unsaturated chain end (PENE) was initially pictured[88,89] as a concerted (but symmetry-disallowed) ($\sigma_2 + \sigma_2$) 1,3-sigmatropic rearrangement, a long-chain free-

Chart 1. Free-Radical Chain Mechanism for PE Degradation

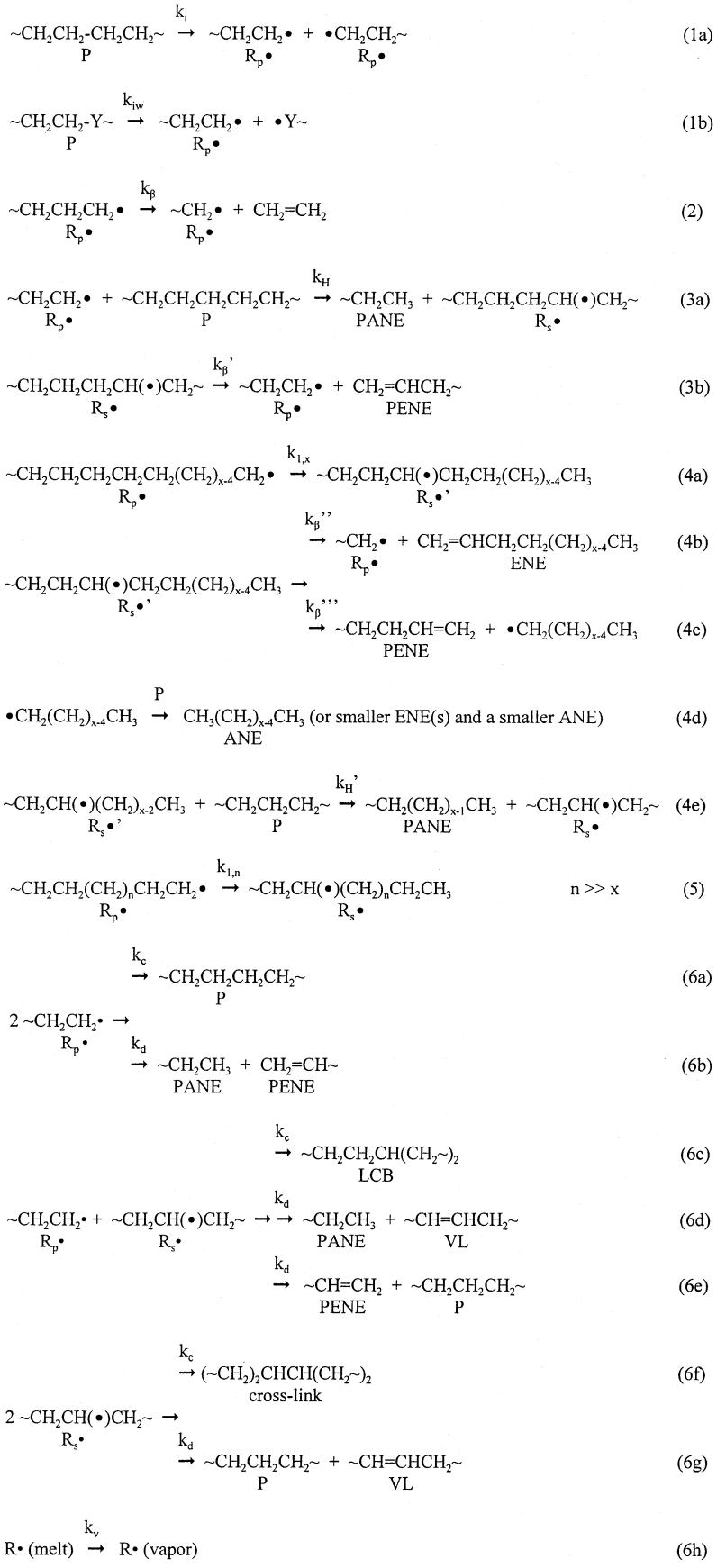

radical mechanism is now accepted[36,90] analogous to that for small hydrocarbons.[91] The usual initiation, propagation, and termination steps are illustrated in Chart 1 for PE.[92] Initiation occurs either by C−C homolysis in the polymer (P) backbone to form *prim* chain-end radicals ($R_p^•$) (step 1a) or by more rapid homolysis of

"weak links" (step 1b).[93] The net rate constant for initiation is $(f)(k_i)$, where f is the fraction of radicals that escape the cage in which they are formed.[94] Cage escape in a viscous polymer melt, probably more by segmental than translational diffusion, will likely increase as MW decreases during pyrolysis,[1f] and the polymer configuration moves from the entangled to the random-coil state.[95,96] However, f will not be simply related to macroscopic melt viscosity and is difficult to predict.[97] Cage recombination achieves no chemical change, but cage disproportionation would give the same stoichiometric result[44] as the "concerted" process noted above and, if $f \ll 1$, could make a nonnegligible contribution to the RS pathway even with a sizable kinetic chain length (KCL).[98]

One propagation pathway available to $R_p^\bullet$ is β-scission to form monomer (the UZ pathway) and regenerate itself, except for a decrease in degree of polymerization (DP) by one (step 2). Second, abstraction of hydrogen from another P chain (intermolecular transfer or simply "transfer") generates PANE and a *sec* on-chain radical ($R_s^\bullet$) (step 3a). Its subsequent β-scission (step 3b) forms PENE and regenerates $R_p^\bullet$ with DP for both reduced, on average, by half.[99] Sequence 3 constitutes the RS pathway. Third, abstraction of hydrogen from the same polymer chain (intramolecular 1,*x*-hydrogen shift or the BB pathway) generates a "near-end" *sec* on-chain radical ($R_s^{\bullet\prime}$) (step 4a). Its β-scission forms either a volatile ENE and $R_p^\bullet$ with modestly reduced DP (step 4b) or PENE with modestly reduced DP and a small alkyl radical (step 4c) which will ultimately be converted to a volatile ANE by transfer (step 4d). However, $R_s^{\bullet\prime}$ can also competitively undergo additional serial 1,*x*-shifts to move the radical center further along the chain (not pictured) or transfer (step 4e) which "cancels" the effect of step 4a. For step 4a, $x = 5$ involving a six-membered-ring transition state is kinetically favored (see below). C−C scissions achieved by step 1a or by sequence 3 are statistically random, but those achieved by steps 2, 4b, and 4c are not. A final, seldom discussed propagation step[86a] would be a 1,*x*-shift *much* further along the polymer chain as an alternative intramolecular route to $R_s^\bullet$ (step 5, large n). Its competition with intermolecular step 3a should depend on long-range polymer conformational factors that can place the radical center in $R_p^\bullet$ adjacent not only to C−H bonds in neighboring P molecules but also to those in its own random coil.

Chains are terminated by radical combination or disproportionation; self-reaction of $R_p^\bullet$ is shown in steps 6a and 6b, cross-reaction of $R_p^\bullet$ and $R_s^\bullet$ in steps 6c−6e, and self-reaction of $R_s^\bullet$ in steps 6f and 6g. Combinations involving $R_s^\bullet$ would introduce LCBs or cross-links into the residual polymer, while disproportionations would generate VL functionality.[100] Radical−radical encounter in a viscous polymer melt is expected to be diffusion-limited, and k_t will likely increase as MW decreases.[1f] Finally, a unimolecular termination mode is sometimes considered in which a small radical evaporates (step 6h) in competition with, e.g., step 4d; this however begs the question of its ultimate product-forming fate downstream.

For long KCL, product distributions depend on the relative propagation rate constants for $R_p^\bullet$ and $R_s^\bullet$ as a function of polymer structure and T but not on k_i and k_t; note that the pseudo-first-order rate constant for transfer is $k_H[M]$, where $[M] = \rho/m_0$ is the concentration of monomer units which is largely invariant during reaction, p is the melt density, and m_0 is the monomer molecular mass. Hence for product predictions, the complex issues of "weak link" vs normal initiation, effects of MW on f and k_t, and ratios of k_{comb}/k_{dispr} can be largely side-stepped.[1b,d,f] For example, if k_β for $R_p^\bullet$ were much greater than $k_H\rho/m_0$ and k_{1x}, step 2 would dominate; for this UZ extreme, the monomer[101] would be evolved from the beginning of the reaction while the MW of the residue would remain largely unchanged[102] because, once a backbone bond broke to form $R_p^\bullet$, that polymer chain would totally unzip to monomer in rapid successive steps. While the minimal selectivity to ethylene clearly indicates that PE does not represent this extreme, vinyl polymers with quaternary centers, such as poly(methyl methacrylate) (PMMA) and poly(α-methylstyrene) (PαMS), do illustrate prototypical UZ behavior.[1] If instead $k_H\rho/m_0$ were much greater than k_β and k_{1x}, the RS extreme by successive repetitions of sequence 3 would dominate; a major initial decrease in MW would result but with a lag time for the generation of volatiles,[102] for which PE gives some evidence. Finally, if k_{1x} were much greater than $k_H\rho/m_0$ and k_β, sequence 4 would intervene; for this BB extreme, immediate formation of volatile ENEs and ANEs larger than monomer would occur with a nonstatistical distribution, for which PE also gives some evidence.

Literature Approaches to Mechanistic Modeling. No mechanistic model exists that fully relates rate constants for the elementary steps shown in Chart 1 to experimental observations, especially product distributions. Various partial models are summarized here and described in more detail in the Supporting Information. These illustrate the complexity of the task and the disparate conclusions that have been reached.

One approach is to deconvolute the global E_{exp} and A_{exp} values derived from TGA data into the contributions from E and A of elementary steps. Unfortunately, the E_{exp} and A_{exp} values are themselves method- and model-dependent.[1b,34a] Additional ambiguity arises because the TGA process does not monitor the entire chemistry outlined in Chart 1 but only that part which forms products small enough to evaporate; on the other hand, the observed rate of weight loss involves both a chemical rate and an evaporation rate. Kinetic expressions for x and changes in the MWD of the residue have been derived[1b,c] by applying the steady-state approximation for various idealized extremes of Chart 1 with assumptions concerning the modes of initiation and termination, the relative contributions of UZ and transfer (BB was not typically included), and the value of L_c. For *simple* chain reactions with bimolecular termination, the steady-state approximation leads to $E_{exp} = {}^1/_2E_i - {}^1/_2E_t + E_{prop}$, where E_{prop} refers to the "rate-limiting" propagation step, i.e., the step that consumes the radical that accumulates to the highest absolute concentration and hence dominates termination.[104] Performing such a deconvolution for polymer pyrolysis is tenuous at best because multiple initiation and termination steps are likely involved, specification of a single "rate-limiting" propagation step is problematical, and volatilization may offer kinetic resistance. However, in a suggestive example of this approach, Dickens[28] assumed that weight loss occurred largely by sequence 3 (no UZ or BB), initiation by allylic end group homolysis, and termination by disproportionation. He then converted a typical TGA value[25d] of $E_{exp} = 62-66$ kcal mol^{-1} into $E_{prop} \approx 31.5$ kcal mol^{-1} by choosing $E_i \approx 72$ kcal mol^{-1}

(reasonable by current estimates; see below) and $E_t \approx 7$ kcal mol^{-1} (from diffusion data in molten PE). Since this E_{prop} value is twice that expected for transfer but reasonable for β-scission (see below), he suggested that β-scission is "rate-limiting", and therefore the dominant termination events will involve $R_s^\bullet$, in contrast with the much more commonly assumed $R_p^\bullet$.

In a more detailed approach to deconvoluting TGA data, Sezgi, McCoy, and co-workers[31a] combined chemical and mass transfer kinetics and applied continuous distribution kinetics and the method of moments. Lumped rate constants were assigned for random scission (k_d), reverse repolymerization (k_a), and "chain-end scission" (k_s, apparently including homolysis, BB, and UZ[31b] as the weight-loss events). Regression of TGA and MWD data at 370−410 °C led to Arrhenius parameters only for the latter: $A_s = 1.14 \times 10^8$ s^{-1} and $E_s = 35$ kcal mol^{-1}; limiting the data to the early t portion only led instead to $A_s = 1.33 \times 10^3$ s^{-1} and $E_s = 20$ kcal mol^{-1}; and an alternate method of data treatment gave $A_s = 1.35 \times 10^6$ s^{-1} and $E_s = 31$ kcal mol^{-1}. Such variable derived Arrhenius values do not assist in mechanistic interpretation of the k_s process. By assigning $A_a = 1 \times 10^5$ M^{-1} s^{-1} and $A_d = A_s = 1 \times 10^{11}$ s^{-1} without detailed justification, Kodera and McCoy[31b] derived corresponding values of $E_a \approx 20$, $E_d \approx 44$, and $E_s \approx 38$ kcal mol^{-1} from early isothermal TGA data of Madorsky[1c] as well as new dynamic TGA data. These Arrhenius parameters were not further related to specific elementary steps, and the authors properly recognized that such a kinetic model is "a simplification of the more detailed radical processes that underlie degradation".[106]

The inverse thermochemical kinetic approach assigns rate constants to the elementary steps based on the behavior of small-molecule models and then attempts to predict the composite behavior. In this regard, Mita[1d] made perceptive semiquantitative observations some 25 years ago and laid a framework for further understanding of the effects of polymer structure. On the basis of estimates of E_β, E_H, A_β, and A_H, he predicted $\bar{\epsilon} \approx k_\beta/k_H$[M], where the "zip length" $\bar{\epsilon}$ is the number of monomer units released from $R_p^\bullet$ before transfer or termination intervenes. The estimate of $\bar{\epsilon} \approx 0.01-0.1$ at 400 °C for PE agrees qualitatively with its minuscule tendency to unzip.[107]

Holmstrom and Sorvik[46b] considered the competitive degradation and formation of LCBs at prevolatilization temperatures and proposed E values for allylic end group homolysis, termination, β-scission, 1,x-shift (both $x = 4$ and 5 portrayed), and transfer of $R_p^\bullet$ of 61.5 (much too low by current estimates; see below), 0 (no diffusional resistance), 26, 10, and 10 kcal mol^{-1} (approximately correct by current estimates; see below), respectively. Hence, the minimal UZ of PE was supposedly rationalized, but none of the equally contributory A factors were estimated. In contrast, Kuroki and co-workers[47a] proposed that termination would be seriously diffusion-restricted, the KCL would therefore be very large, and hence the proposed formation of LCBs by termination step 6c[46b] would be too limited to account for LCB formation (see below for their unusual rationalization).

From isothermal TGA data for HDPE, Bockhorn and co-workers[33a,b] focused on the derived n value that increased from 0.8 to 1.4 over the range 430−480 °C.[108] Their proposed mechanism included steps 1a, 2, 3a, 4a, 6a, and 6b, but it did not distinguish $R_s^\bullet$ and $R_s^{\bullet\prime}$ and lumped step 3b into steps 4b and 4c. They then formulated the volatilization rate as a sum of terms as shown and inserted steady-state expressions for $[R_p^\bullet]$ and $[R_s^\bullet]$ to derive[109]

$$\begin{aligned}
&\mathrm{d[volatiles]}/\mathrm{d}t = \\
&\quad \mathrm{d[C_2H_4]}/\mathrm{d}t + \mathrm{d[alkenes\ from\ step\ 4b]}/\mathrm{d}t + \\
&\quad \mathrm{d[alkanes\ from\ step\ 3a]}/\mathrm{d}t = k_2[R_p^\bullet] + \\
&k_{4b}[R_s^\bullet] + k_{3a}[R_p^\bullet][P] = k_2\{k_{1a}/(k_{6a}+k_{6b})\}^{0.5}[P]^{0.5} + \\
&\quad \{k_{4b}k_{4a}/(k_{4b}+k_{4c})\}\{k_{1a}/(k_{6a}+k_{6b})\}^{0.5}[P]^{0.5} + \\
&\quad \{k_{4b}k_{3a}/(k_{4b}+k_{4c})\}\{k_{1a}/(k_{6a}+k_{6b})\}^{0.5}[P]^{1.5} + \\
&\quad k_{3a}\{k_{1a}/(k_{6a}+k_{6b})\}^{0.5}[P]^{1.5} = C[P]^{0.5} + C'[P]^{1.5}
\end{aligned}$$

The increase of n with increasing T was then interpreted as resulting from a gradual shift from the half-order term associated with 1,x-shift and the formation of ENEs to the three-halves-order term associated with transfer and the formation of ANEs. Several concerns exist with this formulation. First, it improperly decouples the stoichiometry of ANE and ENE formation, because step 4b that produces ENEs occurs in parallel with step 4c that produces ANEs and step 3a that produces ANE functionality is coupled with step 3b that produces ENE functionality. Second, it confuses the n dependences on x and [P] that are not parallel quantities[38] and also confuses $[P] = \rho/M_n$ and $[M] = \rho/m_0$. Third, their product data (Table S3) actually suggest the reverse trend because the initial ANE:ENE ratio decreased with increasing T. Fourth, the authors suggested $E_{1a} = 86$ kcal mol^{-1}, $E_2 = 25.8$ kcal mol^{-1}, $E_{3a} = 10$ kcal mol^{-1}, $E_{4b} = E_{4c} = 26.8$ kcal mol^{-1}, and $E_{6a} = E_{6b} = 0$ kcal mol^{-1}; hence, as the rate supposedly moved from the term dominated by E_{4b} to that dominated by E_{3a}, E_{exp} should have decreased significantly, contrary to their observation of a constant $E_{exp} = 64.1$ kcal mol^{-1}. Ballice[32b] interpreted dynamic TGA data in terms of elementary steps similar to those of Bockhorn but manipulated data in terms of separate first-order expressions for the formation of ANEs and ENEs. The derived Arrhenius parameters for HDPE for formation of ANEs (ENEs) were $A = 6 \times 10^{-2}$ (1.6×10^{-4}) s^{-1} and $E = 9.9$ (29.8) kcal mol^{-1}.[110] Such abnormally low A factors and E values have no mechanistic relevance.

The most detailed thermochemical kinetic treatment was presented recently by Ranzi and co-workers[30a] and Faravelli and co-workers.[30b] They selected k_H and k_β values from gas-phase data for small models (see below). They selected $k_i = 10^{14.9}\exp(-82100/RT)$, $10^{14.9}\exp(-80500/RT)$, and $10^{13.5}\exp(-71500/RT)$ s^{-1} for backbone, branch point, and TV end-group allylic homolysis in the gas phase, respectively (A factors too low by current estimates; see below) but suggested that homolysis would be *accelerated* some 50-fold in the polymer melt because of a reduction in E of 5.3 kcal mol^{-1} attendant on transposition from the gas to the condensed state.[103b,111] However, experimental data on model compounds do not support such a significant phase difference for homolysis rate constants, once cage effects are properly considered.[112] They assigned a diffusion-limited $k_t = 10^{10.4}(T/400)\exp(-5960/RT) = 4.8 \times 10^8$ M^{-1} s^{-1} at 400 °C for $R_p^\bullet$. Their initial simulation of TGA data[30a] did not include BB because they felt that 1,x-shifts would be significantly restricted in the melt. Stoichiometric balance equations for RS were formu-

lated as $ANE_n \rightarrow ENE_j + ANE_{n-j}$; $ENE_n \rightarrow 0.5(DIENE_j + ANE_{n-j}) + 0.5(ENE_j + ENE_{n-j})$; and $DIENE_n \rightarrow DIENE_j + ENE_{n-j}$. Each ANE_n, ENE_n, and $DIENE_n$ was consumed by sequence 3 and formed analogously from larger species, with n truncated at ≤2000 carbons and a Schulz−Flory distribution assumed for the initial ANE polymer. To allow numerical simulation,[30a] the key simplification, based on the estimated inequality $k_\beta \ll k_H(\rho/m_0)$, was use of a *single* "rate-limiting" propagation rate constant, i.e., $k_{rds} \approx k_\beta\{k_H(p,s)/k_H(s,s)\}\{m_0/\rho\}[R_p^\bullet]$ with $[R_p^\bullet] \approx \{2k_i(p,p)/k_t\}^{1/2}\{\rho/m_0\}^{1/2}$ from the steady-state approximation.[113,114] The predicted TGA profiles fell between those of the two experimental data sets chosen, which disagreed significantly between themselves. While the authors considered such agreement to be "quite good", they did not present any sensitivity analyses for the estimated rate constants, especially for the "accelerated" value used for k_i or the estimated L_c value based on T and pressure (see also below). This model was later expanded[30b] to include TV end-group allylic homolysis and BB (with $k_{15} > k_{16} > k_{14}$ and apparent removal of its restriction to the gas−liquid interface).[115] Also, a restrictive rate term for mass transfer of volatiles ($n < L_c$) via bubble formation was added, since volatilization was postulated to occur only at the gas−liquid interface rather than by bulk diffusion. The expanded model predicted with reasonable success the observed distribution profiles of major ENE products vs c (Table S4), but no predictions were presented for ANEs or DIENEs which were not reported but which, as noted below, seldom conform to the idealized ANE:ENE:DIENE = 1:2:1 ratio assumed in the balance equations. The differences in predicted TGA profiles with and without the added "resistance to volatilization" term were at least as great as the differences between prediction and experimental data. Thus, the complexity of adding BB and a rate-retarding role of mass transfer appears to compromise the significance of the degree of agreement reached with the simpler model.[30a] These studies vividly illustrate the challenge in constructing a mechanistic model for the entire course of a polymer pyrolysis reaction.

Stoichiometry Results and Issues

Expectations. Regardless of mechanism, stoichiometric constraints exist, to which much of the existing product data does not conform well. The UZ pathway to form monomer is obviously stoichiometrically balanced. For the RS pathway, if we ignore the trivial effects of end groups in a high-MW polymer, steps 3a and 3b produce new PANE and PENE chain ends in equivalent amounts:

$$\sim(CH_2)_nCH_2(CH_2)_n\sim \rightarrow \sim(CH_2)_{n-2}CH_3 + \sim(CH_2)_nCH{=}CH_2$$

Repetition for large KCL until volatile fragments are formed, with both directionalities for step 3b allowed, will produce a 1:2:1 statistical ratio of volatile ANEs:ENEs:DIENEs[30a,63b,72b,85] for each c value. The stoichiometry of the BB pathway is more complex because, in contrast to UZ and RS, it cannot occur exclusively; its stoichiometry is coupled with RS since the production of alkyl radicals in steps 4b and 4c must ultimately lead to transfer in steps 3a and 4d:

$$\sim(CH_2)_{n+2}CH_2(CH_2)_{x-2}CH_2^\bullet \rightarrow \sim(CH_2)_{n+2}CH(^\bullet)(CH_2)_{x-2}CH_3$$

$$^1/_2\sim(CH_2)_{n+2}CH(^\bullet)(CH_2)_{x-2}CH_3 \rightarrow {}^1/_2CH_2{=}CH(CH_2)_{x-2}CH_3 + {}^1/_2\sim(CH_2)_nCH_2^\bullet$$

$$^1/_2\sim(CH_2)_{n+2}CH(^\bullet)(CH_2)_{x-2}CH_3 \rightarrow {}^1/_2\sim(CH_2)_{n+2}CH{=}CH_2 + {}^1/_2CH_3(CH_2)_{x-4}CH_2^\bullet$$

$$^1/_2\sim(CH_2)_nCH_2^\bullet + {}^1/_2\sim(CH_2)_{n+2}CH_2(CH_2)_n\sim \rightarrow {}^1/_2\sim(CH_2)_nCH_3 + {}^1/_2\sim(CH_2)_{n+2}CH(^\bullet)(CH_2)_n\sim$$

$$^1/_2CH_3(CH_2)_{x-4}CH_2^\bullet + {}^1/_2\sim(CH_2)_{n+2}CH_2(CH_2)_n\sim \rightarrow {}^1/_2CH_3(CH_2)_{x-4}CH_3 + {}^1/_2\sim(CH_2)_{n+2}CH(^\bullet)(CH_2)_n\sim$$

$$\sim(CH_2)_{n+2}CH(^\bullet)(CH_2)_n\sim \rightarrow \sim(CH_2)_{n+2}CH{=}CH_2 + \sim(CH_2)_{n-2}CH_2^\bullet$$

$$\sum:\ \sim(CH_2)_{n+2}CH_2(CH_2)_{x-2}CH_2^\bullet + \sim(CH_2)_{n+2}CH_2(CH_2)_n\sim \rightarrow \sim(CH_2)_{n-2}CH_2^\bullet + {}^1/_2CH_2{=}CH(CH_2)_{x-2}CH_3 + {}^1/_2CH_3(CH_2)_{x-4}CH_3 + {}^3/_2\sim(CH_2)_{n+2}CH{=}CH_2 + {}^1/_2\sim(CH_2)_nCH_3$$

While the propagating $R_p^\bullet$ has necessarily lost $(x + 3)$ CH_2 groups in this cycle, this equation is otherwise chemically balanced and can be summarized as

$$P \rightarrow {}^1/_2ANE + {}^1/_2ENE + {}^1/_2PANE + {}^3/_2PENE$$

Hence, the initial volatiles should be H-rich (ANE = ENE but no DIENE) with the H:C stoichiometry balanced by the simultaneous production of more unsaturated than saturated chain ends in the residue (PENE > PANE). Thus, preferential BB at low x could produce volatiles consisting of ANEs and ENEs without DIENEs[63b,72b] before the fragments from the coupled RS component fell below L_c. However, the residue would be simultaneously accumulating "excess" unsaturated end groups ($f_t > 1$), and hence the RS products should have DIENEs > ANEs as the residue becomes increasingly H-poor. The cumulative equality ANE = DIENE is ultimately demanded at $x = 1$, unless weight loss is incomplete and a C-rich residue remains.

Data. The ideal ratio of ANE:ENE:DIENE = 1:2:1 expected for RS is seldom, if ever, observed experimentally. Even the less restrictive ANE = DIENE balance required at $x = 1$ if there is no final residue is seldom realized. In the low-T regime, only traces of DIENEs are reported (Tables S2 and S3), and the consistent pattern of ANE ≫ DIENE represents an excess of H in the volatile products. Yet, at least in the early stages of pyrolysis, reported f_t values for the residue are 1 *or less*;[42,47,49] i.e., it is also H-rich. We are not aware of reports of the production from PE at partial conversion of H-poor nonvolatile telechelic oligomers with a majority of PENE end groups ($f_t > 1$), although these have been reported from polypropylene[116] and polyisobutylene.[117] Thus, the very low proportion of volatile DIENEs produced in the low-T regime even at high x, coupled with the typical absence of a C-rich residue,[35c] poses an

Table 1. Estimates of Rates of Initiation Processes as a Function of M_n and y_{br}[a]

process	model reaction	rate expression ($M\ s^{-1}$)[b]	relative rate at T = 400 °C and M_n = [c] 1×10^6	1×10^5	1×10^4	1×10^3
(a) homolysis: backbone	butane[d] → 2 ethyl[e,f]	$\{10^{17.4} \exp(-86300/RT)\}\{2[M]\}$[g]	1.0 1.0	1.0 1.0	1.0 1.0	1.0 1.0
(b) homolysis: branch point (model 1)	2-methylbutane[d] → ethyl + 2-propyl[e,f]	$\{10^{17.6} \exp(-85100/RT)\}\{3y_{br}\}\{2[M]\}$[h]	0.3 0.01	0.3 0.01	0.3 0.01	0.3 0.01
(b′) homolysis: branch point (model 2)	3-ethylpentane[d] → ethyl + 3-pentyl[f,i]	$\{10^{17.7} \exp(-83400/RT)\}\{3y_{br}\}\{2[M]\}$[j]	1.3 0.05	1.3 0.05	1.3 0.05	1.3 0.05
(c) homolysis: TV end group	1-pentene[d] → ethyl + allyl[k,l]	$\{10^{16.4} \exp(-73100/RT)\}\{f_t[P]\}$[m]	0.03 0.03	0.3 0.3	2.7 2.7	27 27
(d) MD: backbone + TV end group	butane + 1-butene[d] → 2 2-butyl[e,f]	$\{10^{11.6} \exp(-62000/RT)\}\{4[M]\}\{f_t[P]\}$[n]	0.2 0.2	1.6 1.6	16 16	160 160
(e) MD: TV end group + TV end group	2 1-butene → 2-butyl + 1-methylallyl[o]	$\{10^{9.4} \exp(-48100/RT)\}\{2f_t[P]\}\{f_t[P]\}$[p]	0.0 0.0	0.05 0.05	4.6 4.6	460 460
total rate; model 1 ($M\ s^{-1}$)			1.6×10^{-9} 1.3×10^{-9}	3.5×10^{-9} 3.2×10^{-9}	2.7×10^{-8} 2.6×10^{-8}	7.0×10^{-7} 7.0×10^{-7}
total rate; model 2 ($M\ s^{-1}$)			2.7×10^{-9} 1.3×10^{-9}	4.6×10^{-9} 3.2×10^{-9}	2.8×10^{-8} 2.6×10^{-8}	7.0×10^{-7} 7.0×10^{-7}

[a] Assume $f_t = 1$. [b] [M] = concentration of monomer units = $1000\rho/28$; [P] = concentration of polymer = $1000\rho/M_n$; y_{br} = fraction of backbone carbons that are branched; f_t = number of TV end groups per molecule; ρ = melt density, taken as 0.644 g/mL at 400 °C (see text); E values in cal mol^{-1}. [c] Upper line: $y_{br} = 0.025$ (typical of LDPE); lower line: $y_{br} = 0.001$ (typical of HDPE). [d] $\Delta H_f°_{298}$, $S°_{298}$, $C_p°_{298}$, and $C_p°_{800}$ from ref 120a. [e] $\Delta H_f°_{298}$ from ref 120b. [f] $S°_{298}$, $C_p°_{298}$, and $C_p°_{800}$ from ref 120c. [g] k_{comb}(ethyl) = $1.08 \times 10^{10}\ M^{-1}\ s^{-1}$ (ref 121d). [h] k_{comb}(ethyl + 2-propyl) = $1.12 \times 10^{10}\ M^{-1}\ s^{-1}$ (ref 121a). [i] $\Delta H_f°_{298}$ from ref 120c. [j] k_{comb}(ethyl + 3-pentyl) assumed same as k_{comb}(ethyl + 2-propyl). [k] $\Delta H_f°_{298}$ from ref 120d. [l] $S°_{298}$, $C_p°_{298}$, and $C_p°_{800}$ from ref 122. [m] k_{comb}(ethyl + allyl) = $2.23 \times 10^{10}\ M^{-1}\ s^{-1}$(ref 121c). [n] k_{dispr}(2-butyl) ≈ $5.0 \times 10^8\ M^{-1}\ s^{-1}$, estimated as that for 2-propyl (ref 121a) multiplied by 1/4 for reaction path degeneracy. [o] $\Delta H_f°_{298}$, $S°_{298}$, $C_p°_{298}$, and $C_p°_{800}$ taken as average of valence bond structures, estimated from ref 122. [p] k_{dispr}(2-butyl + 1-methylallyl) assumed same as k_{dispr}(2-butyl).

unaddressed apparent violation of H:C stoichiometry. Any hypothesis that DIENES are rapidly converted to other (unidentified and undetected) products is weakened by the fact that DIENES do survive as significant products at much higher T (see below). Some authors have reported formation of H-poor aromatics at high x,[32,73] but there are several reports to the contrary.[33a,c]

The composite ANE:ENE ratios reported for the low-T regime (Table S3) are seriously inconsistent, ranging from >3 for C_{1-30}[33] to <1 for C_{3-28}[72] with varying values in between.[33a,c,64,66b,71,75] GC data suggest that the ANE:ENE ratio increases with increasing c,[32,33a,c,66b,75] but the magnitude of the trend ranges from sizable[32] to modest.[75] (There is also indication that this ratio increases with increasing x.[64]) However, if the FIMS data[78] are quantitatively correct, then this trend must dramatically reverse at still higher c, although issues concerning calibration and inconsistencies with overlapping GC data have been noted above. A trend for the ANE:ENE ratio to increase with increasing c might indeed result if initially formed larger ENEs were more rapidly degraded to smaller ENEs than are initially formed ANEs.[13b,64] However, correspondingly low ANE:ENE ratios should then be observed at low c; yet the data in Figure 1 reveal ANE:ENE ratios for the light hydrocarbons that remain near unity.

In the high-T regime (Table S4), DIENEs do become significant products. Reported ANE:ENE ratios range from < 0.5[6a,22,58a,74,85,87] to near 1[85,86a] and appear to decrease modestly with increasing T[74] but do not appear as dependent on c as at lower T. Inversely, DIENE:ENE ratios appear to increase significantly with increasing T[67,74,86a] and also to increase modestly with increasing c.[6a,b,67a,85,87] The stoichiometrically significant ANE:DIENE ratio, ideally 1:1, thus decreases with increasing T. For example, Wampler and Levy[67a] reported ratios for the C_{13-17} fraction that decreased from 3 to 5 at 600 °C to 0.6−0.7 at 1000 °C, with ENEs always dominant.[118a] Blazso and co-workers[74] reported the same trend as the ANE:ENE:DIENE ratio for the composite C_{9-32} fraction changed from 51:46:≈3 to 27:59:15 to 14:57:29 at 400, 600, and 800 °C, respectively. This ANE:DIENE ratio also appears to decrease to a lesser extent with increasing c, but absolute values are not consistent. For example, for HDPE over similar ranges of C_{10-20}, the ratio decreased from ≈1 to <1 with increasing c at both 650[87] and 1000 °C,[85] but from <1 to ≪1 at the intermediate 768 °C.[6a] In a GC study at 510 °C limited to analysis of C_{10-},[118b] ANE:ENE:DIENE ≈ 1:2:1 was reported for C_9 but ENE > ANE ≫ DIENE for C_{7-8}. Thus, no data set at high T allows construction of a total H balance for the composite volatiles.

Observations on Mechanistic Issues

Initiation and Kinetic Chain Length. Initiation likely involves multiple processes whose composition changes as degradation proceeds. In addition to homolysis of backbone C−C bonds (step 1a), homolysis of weaker minority bonds (step 1b),[119] particularly the significantly weaker allylic C−C bonds adjacent to unsaturation[28,31a,46b,47a,49,50,56,57a,63a] and/or the somewhat weaker C−C bonds at branch points,[31a,43,49,50,53,63a] has been commonly considered. Weak-link scission has been suggested to rationalize the greater thermal lability of PE compared with large n-alkanes.[42,46b,49] In no case, however, does either the ratio k_{1b}/k_{1a} or the KCL appear to be known quantitatively for a given PE as a function of conditions.

Thermochemical kinetic estimates[120−122] for homolysis rates based on simple model systems at 400 °C, near the onset of PE volatilization, are collected in Table 1 for various values of M_n and y_{br}, the fraction of backbone carbons that are branched. Homolysis of butane, step a, models backbone cleavage, and the relative rates of other processes are compared to it in Table 1. Homolysis of 2-methylbutane, step b, is the simplest model for

cleavage at a branch point (note that each branch generates three weakened bonds). However, this may be too simple a model because it does not contain the full accumulation of local destabilizing gauche interactions about a branch point in PE. We therefore also consider homolysis in 3-ethylpentane, step b′, which is predicted to be almost 5-fold more rapid than in 2-methylbutane per equivalent $C_{sec}-C_{tert}$ bond. For a typical HDPE with $y_{br} = 0.001$, homolysis at branch points is thus predicted to be noncompetitive, but for a typical LDPE with $y_{br} = 0.025$, it becomes comparable in rate to that in the backbone. Homolysis of 1-pentene, step c, is the simplest model for cleavage at a TV end group (similar models could be developed for VD and VL sites). Since the rate of end-group homolysis is dependent on [P] rather than [M], it will scale as M_n^{-1}. Thus, as degradation progresses and M_n decreases while f_t remains near 1, end-group homolysis is predicted to become increasingly competitive with backbone and branch-point homolysis. The estimates in Table 1 predict a crossover at $M_n \approx 15\,000$, below which end-group homolysis would dominate. This estimate is likely a conservative lower limit since the fraction of cage escape of the small allyl radical is likely larger than for polymeric radicals.

However, in addition to these typically considered homolysis reactions, there may be significant initiation by molecular disproportionation (MD).[104b,123] While this process of donation of H from a C−H bond to an unsaturated linkage to form two radicals is well-recognized in thermal reactions of olefins and aromatics, especially under condensed-phase conditions that favor bimolecular processes, it has not been considered in the polymer pyrolysis literature, even though it is clear that the concentration of olefinic termini in the degrading polymer increases with increasing x and decreasing M_n. Reaction of butane with 1-butene, step d, was chosen to model MD of a backbone C−H bond and a TV end group. Self-reaction of 1-butene, step e, was chosen to model MD of an allylic C−H bond at a TV site and a TV end group. The rate of step d, which shares a M_n^{-1} dependence with step c, as well as the same f_t dependence, is predicted in fact to be some 6-fold *more* rapid. Hence, bimolecular MD of a TV end group with a backbone C−H bond may well be as important an initiation step as unimolecular end-group homolysis under all conditions. The rate of step e scales as M_n^{-2} and thus, while a trivial contributor at high M_n, is predicted to dominate all initiation pathways at the lowest M_n. Although the estimates in Table 1 are approximate, they strongly suggest that the MD process cannot be ignored, and thus the mixture of initiation pathways may be even more complex than typically considered. In summary, initiation at high M_n is predicted to be dominated by backbone and, for branched PE, branch-point homolysis, but initiation at low M_n is predicted to be dominated by the MD processes. As T increases, the relative contributions from pathways a−e should increase in the order of their increasing E values, i.e., (a) ≥ (b/b′) > (c) > (d) > (e). The total estimated rate of radical formation from all processes increases significantly as M_n decreases and hence should do the same as x increases during a degradation.

To compare these estimates of initiation rates to the behavior of PE in the T regime below the onset of volatilization but above that of "enlargement", we converted 21 data points[44,47,49] (T = 338−390 °C and M_{n0} = 10 700−29 500) on MW reduction in a Phillips HDPE, which should have ≈1 TV group/molecule, minimal branching, and negligible peroxide content, into $k_{MW} = 14[(1/M_{nt}) - (1/M_{n0})]/t$ values.[1a,c,52] We assign no mechanistic significance to the derived Arrhenius parameters because of *serious* scatter but used them to extrapolate an approximate value at 400 °C of $k_{MW} \approx 1 \times 10^{-6}$ s^{-1}. Hence for illustration, to achieve an $\alpha = k_{MW}t$ value of 0.001 for the probability of breaking any given backbone bond would require 1×10^3 s. Yet in this time period, the probability of bond breaking in the butane model in Table 1 would be only 0.000 000 024, i.e., $([A]_0 - [A])/[A]_0 = 1 - \exp(-k_{homo}t)$. Even given the additional sources of initiation suggested by Table 1, this major disparity, which would be further exacerbated by $f < 1$ for cage escape, suggests that long kinetic chains are required to rationalize the decreases in MW that occur in this T range (cf. Table S1).[124,125]

The occurrence of a "fast" followed by a "slow" stage in the decrease of MW under mild conditions (see above) has often been proposed to indicate a role for (unidentified) weak links that are rapidly consumed in the early stages of degradation.[42,50,53] Yet allylic C−C bonds are not a viable candidate because their concentration in the residue increases with time (see above).[28] Branch points are also a questionable candidate because of the net increase of LCBs under mild conditions (see above). An alternate and more attractive explanation[44] is that the rate decreases as degradation increases, even though the rate of initiation likely increases (Table 1), because decreases in viscosity will strongly accelerate the diffusion-controlled k_t processes;[1f] such an increase in k_t would be reinforced by the increasing diffusivity of the polymer radicals that are steadily decreasing in average size (see below).[126a]

Termination. As just noted, the rate of termination likely increases steadily during degradation, and the relative contributions from various radicals also probably change. The impact of diffusional resistance on the value of k_t has been discussed earlier by Mita and Horie,[1f,126b] but its functional dependence on the MWD, and hence on the extent of degradation, must be complex and is still not quantitatively known. A summary of more recent speculations based on the transition[127] from Rouse[128] to reptation chain dynamics[95,96] and its effects on chain mobility and diffusion is given in the Supporting Information.[129−138]

The common assumption has been that $R_p^\bullet$ is the major terminating species. Yet the estimated inequality $k_\beta < k_H(\rho/m_0)$ (see above and below) suggests that $[R_s^\bullet] > [R_p^\bullet]$, such that $R_s^\bullet$ should dominate termination (unless it suffers significantly greater diffusional constraints than $R_p^\bullet$; see next paragraph).[28] A further seldom addressed issue is the role of allylic on-chain radicals formed by favorable hydrogen abstraction at TV, VL, or VD sites. Since their propagation reactions will be significantly slower than those of $R_s^\bullet$ or $R_p^\bullet$, they may well accumulate to concentrations high enough to participate in the more structure-insensitive termination events.

Random Scission. *DTG Profiles.* Differential thermogravimetric (DTG) plots (dx/dt vs x or t) for the RS pathway should show an initial positive slope toward a maximum because reaction time must accumulate to allow the multiple scissions required to generate fragments with MW < L_c,[1,139a] whereas the UZ and BB pathways should lead to uniformly negative slopes.

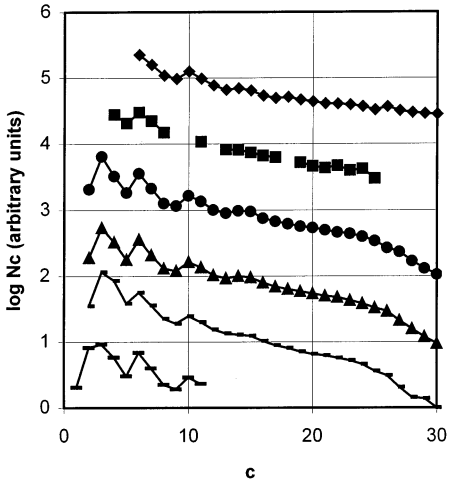

Figure 2. Distributions of total volatiles (N_c) by carbon number (c) from high-T exhaustive flash pyrolyses of PE: ♦, Ziegler HDPE, ≤780 °C, ref 9; ■, Ziegler HDPE, ≤800 °C, ref 86a; ●, Ziegler HDPE, ≤680 °C, ref 58a; ▲, Phillips HDPE, ≤680 °C, ref 58a; −, LDPE, ≤680 °C, ref 58a; —, Ziegler HDPE, 500 °C, ref 57. Ordinates offset by arbitrary amounts for clarity.

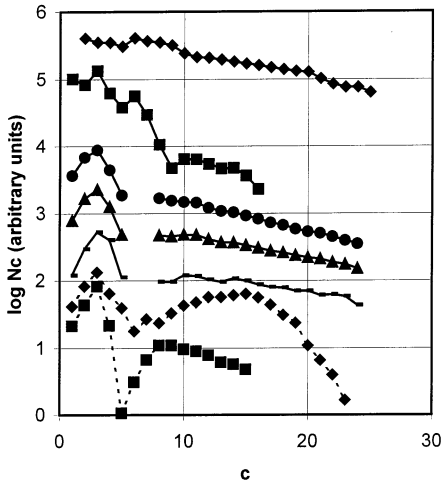

Figure 3. Distributions of total volatiles (N_c) by carbon number (c) from low-T pyrolyses of PE: solid line ♦, LDPE, 420 °C, 30 min, ref 75; solid line ■, PM, 437 °C, 20 min, ref 63; solid line ●, HDPE, 420 °C, 150 min, ref 64; solid line ▲, HDPE, 420 °C, 90 min, ref 64; solid line −, HDPE, 420 °C, 30 min, ref 64; dashed line ♦, HDPE, 420 °C, 15 h, ref 65; dashed line ■, LDPE, 400 °C, >420 min, ref 73. Ordinates offset by arbitrary amounts for clarity.

Typical DTG profiles[25d,43,139b−144] do indeed show maxima at $x \approx 0.3$ for HDPE, but maxima are less pronounced or absent for LDPE. The somewhat more rapid initial rates and lack of maxima for LDPE have typically been attributed to its greater number of branches considered to be weak links and sources of volatile RS fragments early in the reaction, although Wall and Strauss[143] proposed that branches alone could not explain the lack of a maximum and invoked some preference for BB compared with RS in LDPE (see below).

Log N_c−c Plots and the s Parameter. Using various protocols to address the successive cleavages characteristic of RS, several authors have derived as a diagnostic test the proportionality, expressed here for PE: $N_c \propto (1 - s)^{(c-1)}$,[1c,35a,86,145−147] where N_c is the mole fraction of all products (ANEs, ENEs, and/or DIENEs) containing c carbon atoms, s is the probability of cleaving any given C−C bond, and $(1 - s)$ is the probability of that bond remaining intact.[148,149] Hence, a linear plot of log N_c vs $(c - 1)$, or c, is considered diagnostic of RS, whereas specific positive deviations are diagnostic of contributions from nonstatistical mechanisms. The parameter $s \equiv (1 - 10^m)$, where m is the slope. The essence of this relationship is that the formation of a fragment with c carbon atoms requires that its $(c - 1)$ contiguous bonds remain uncleaved.

Data from Tables S2−S4 are plotted in this format in Figure 2 for higher-T data ($x \approx 1$) and in Figure 3 for lower-T data (x typically <1) for those entries which provide quantitative data over a significant c range. Near-linear portions typically occur in the range $c \approx 12$−25. Falloffs at higher c have generally been assumed to result from irreversible losses during GC analysis. Selective maxima above the correlation line at lower c have been taken as evidence for nonstatistical BB, superimposed on a RS background. To characterize the degree of alternation between maxima and minima, we empirically define a single-valued "variability" parameter $v \equiv \langle|\log N_{c+1} - \log N_c|\rangle$, the average of the absolute values of the successive changes in log N_c for $c = 3$−20. The parameter v has its minimum value for pure RS of $|\log(1 - s)|$, e.g., 0.027−0.046 for $s = 0.06$−0.10, and increases as nonstatistical alternation increases. The m, s, and v parameters corresponding to Figures 2 and 3 are compiled in Table 2.

Table 2. Parameters for log N_c−c Plots in Figures 2 and 3

plot[a]	T (°C)	x	m	s	v	ref
2, 1	≤780	≈1	−0.022 to −0.027[b]	0.05−0.06[c]	—[d]	9
2, 2	≤800	≈1	−0.032[b]	0.07[c]	—[e]	86a
2, 3	≤680	≈1	−0.033[f]	0.073[f]	0.115[f]	58a
2, 4	≤680	≈1	−0.037[f]	0.081[f]	0.110[f]	58a
2, 5	≤680	≈1	−0.041[f]	0.090[f]	0.102[f]	58a
2, 6	500	≈1	—[g]	—[g]	—[g]	57
3, 1	420	0.3	−0.047[h]	0.102[h]	0.044[h,i]	75
3, 2	437	<0.1	—[j]	—[j]	—[j]	63
3, 3	420	0.32	−0.044[h]	0.096[h]	—[k]	64
3, 4	420	0.20	−0.034[h]	0.076[h]	—[k]	64
3, 5	420	0.05	−0.025[h]	0.056[h]	—[k]	64

[a] First number is Figure number; second is the plot number in descending order from top; plot 6 in Figure 3 appears anomalous. [b] Back-calculated from authors' value of s. [c] Value given by authors. [d] Lack of data for $c < 6$ precludes calculation. [e] Data gaps for $c = 9$, 10, and 12 preclude calculation. [f] From our plot of authors' data; m for $c = 16$−24. [g] Lack of data for $c > 11$ precludes calculation. [h] From our plot of authors' data; m for $c = 16$−23.[i] $v = 0.046$ for totally RS with $s = 0.010$. [j] Lack of data for $c > 16$ precludes calculation. [k] Data gaps for $c = 6$ and 7 preclude calculation.

Seeger and Gritter[9] derived $s = 0.05$−0.06 from the most extensive data set which involved flash pyrolyses of Ziegler HDPE at ≤780 °C. (An additional near-linear section extending to $c = 40$ is not shown.) Seeger and Cantow[86a] derived $s = 0.07 \pm 0.01$ from an analogous prior study at ≤800 °C. We derived $s = 0.07$, 0.08, and 0.09 respectively from graphical data of Cantow and coworkers[58a] for parallel flash pyrolyses of Ziegler PE, Phillips PE, and LDPE at ≤680 °C. Although the more branched LDPE gave relatively greater amounts of $c = 3$−5 products, lesser amounts of $c > 12$ products, and hence a slightly larger s value than did the HDPEs, the overall variation in s values is modest. The v values derived from these parallel studies are also similar (≈0.11; Table 2). Since data from van Schooten and Evenhuis[57] for flash pyrolysis of HDPE at 500 °C (limited results for LDPE are similar) is limited to $c \leq$

Table 3. Dependence of Parameters on *x* for HDPE in a Closed System at 420 °C[a]

loading (mg)	12.2−12.3			19.9−20.2			27.6−28.1		
x^b	0.04	0.21	0.34	0.05	0.23	0.36	0.04	0.20	0.32
s^c	0.057	0.064	0.092	0.072	0.066	0.088	0.056	0.076	0.096
v^{*d}	0.07	0.05	0.08	0.09	0.05	0.07	0.07	0.06	0.07

[a] Reference 64; system had significant gaseous headspace, which adds some ambiguity to the meaning of the *s* parameter. [b] Based on detected products through C_{24}; increasing *x* values for each loading correspond to $t = 30$, 90, and 150 min. [c] Based on C_{16-23} except C_{16-22} for fourth data column. [d] Based on C_{8-23} except C_{8-22} for first data column; note that v^* is different from the *v* parameter which is normally based on C_{3-20}.

11, *s* and *v* values cannot be calculated, but the pattern at low *c* (Figure 2) is visually very similar to the Cantow data.[58a,150]

In contrast with Figure 2, the plots in Figure 3 for lower-*T* data show serious inconsistencies. Data from Watanabe and co-workers[75] for LDPE in a sealed reactor at 420 °C for 30 min ($x = 0.30$) show a linear regime with a similar slope, i.e., $s = 0.10$, only slightly larger than those in Figure 2, but very little alternation, i.e., a *v* value much lower than typical of Figure 2. Data from Murata and co-workers[19] for HDPE in a CSTR configuration at 420 °C also show very little alternation, although their mode of GC data presentation precludes our including it in Figure 3 in quantitative form. In contrast, data from Tsuchiya and Sumi[63] for PM at 437 °C for 20 min at low *x* in an open system (patterns for HDPE at 375 and 425 °C were very similar) show peak alternation in the low-*c* regime and a more rapid falloff at modest *c*, although the data do not extend to high enough *c* to allow calculation of *s* and *v* values. (Attempted rationalization based on HDPE−LDPE differences would run counter to the suggestion of Wall and Straus[143] that LDPE should be more susceptible to BB.) Of intermediate character are data from De Witt and Broadbelt[64] for HDPE in sealed ampules at 420 °C which include variation in *t* and hence *x*; that for the highest sample loadings, and hence smallest volume ratio of gaseous headspace to melt, is shown in Figure 3; results for lower loadings are very similar except more scattered. A modest general pattern of increasing *s* with increasing *x* for the whole data set (Table 3) is consistent with the increase in bond breaking expected for RS. Although a maximum is evident for $c = 3$, *v* values cannot be calculated because of a data gap for the critical $c = 6-7$ region; modified, less diagnostic v^* values for the $c = 8-23$ region are shown in Table 3. In further contrast, exhaustive pyrolysis data at 420 °C from Jalil[65] in an open system (we combined reported data for gas and liquid fractions to construct the plot shown) show no linear portion and a minimum at $c = 6$. An experimentally similar study at 400 °C by Ohkita and co-workers[73] shows a still different pattern with a deep minimum at $c = 5$. Both these data sets appear atypical in that a significant residue remained, even when volatiles were no longer being produced, and the "oils" in the latter case[73] were significantly branched.

Increasing *T* for flash pyrolysis of Ziegler HDPE over the 640−920 °C range[58a] (data not shown in Figure 2) led to a larger *s*, i.e., smaller average product size, and a smaller *v*, i.e., less distinct maxima at the lower *c* values. In contrast, two reports for the lower-*T* regime suggest a larger average product size as *T* increased. For the condensable volatile material (84−94% yield) from pyrolysis of LDPE in an open stirred reactor with minimal N_2 sweep gas, Park and co-workers[15] reported that its smoothed simulated distillation curve became broader and moved to slightly higher MW as *T* was increased over the range 440−500 °C (132−40 min),

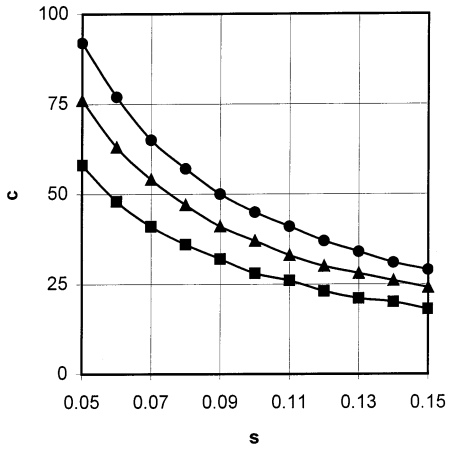

Figure 4. Maximum carbon number (*c*) required to encompass various specified wt % of total volatiles as a function of *s* for idealized RS statistics: ●, 95%; ▲, 90%; ■, 80%.

while its fraction with $c \leq 11$ simultaneously decreased from 29 to 15%. Data for *T*-programmed pyrolyses from Wampler and Levy[67a] also suggest that the average volatiles became larger as the heating rate was increased, and hence the "average *T*" increased,[118a] over the range 5−60 °C/min. These superficially conflicting reports may result from opposing effects of increasing *T*: accelerating successive RS reactions but also increasing L_c, especially in the low-*T* regime.

All data in this section from which *s* values have been derived are from GC analyses limited to $c \leq 40$. The log N_c−*c* relationship cannot be quantitatively tested for the higher-*c* products that are implied qualitatively by the FIMS and fluidized-bed data noted above. Consider the implications for total product distribution of a linear RS relationship over a broader *c* range. Figure 4 displays the upper limit of *c* required to encompass 80, 90, and 95 wt % of the RS products as a function of *s*. For example, for a typical $s = 0.08$ derived from the GC range (Table 2), GC detection limited to $c = 36$ would miss 20 wt % of products with larger *c*, while detection even through $c = 57$ will still miss 5 wt %. For much lower *s* at lower *x*, say $s = 0.03$, 20 wt % of products would remain in the $c \geq 100$ range. Thus, the FIMS results at low *x* might be rationalized if the technique is particularly insensitive to low-*c* material.

Critique of the s Parameter for Open Systems. The derivations of the log N_c−*c* relationship implicitly assume a *closed* system in which all degraded products remain subject to further cleavage, and the parameter *s* constitutes a progress variable for decomposition.[35a] Yet the relationship has been most typically used (Figure 2 and second entry in Figure 3) without comment for the volatile products from *open* pyrolysis systems from which intermediate-sized products evaporate and thus are protected from further cleavage; in this case the applicability of the relationship must be questioned. While considerations of the kinetics of

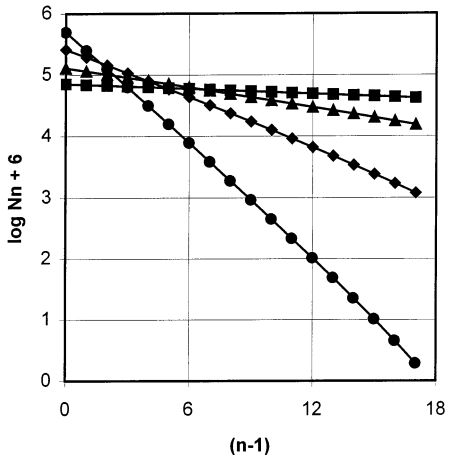

Figure 5. Simulated distributions of products (N_n) in the melt from RS of P(19) as a function of DP(n) for $k_{evap} = 0$ for all products (closed system), with specified wt % conversions to $n = 1-9$ products: ■, 10 wt %, $s = 0.03$; ▲, 40 wt %, $s = 0.12$; ♦, 80 wt %, $s = 0.27$; ●, 99 wt %, $s = 0.52$.

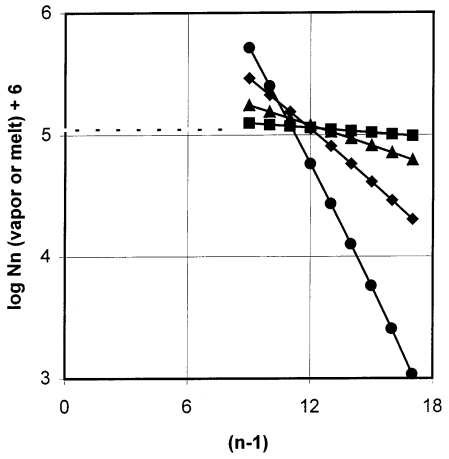

Figure 6. Simulated distributions of products (N_n) in the melt (solid lines) and in the vapor (dashed line; same results for all conditions) from RS of P(19) as a function of DP(n) for $k_{evap} = 0$ for $n = 10-18$ but 1×10^6 for $n = 1-9$ (open system with sharp discontinuity at $L_n = 9$), with specified wt % conversions to $n = 1-9$ products: ■, 10 wt %, $s = 0.03$; ▲, 40 wt %, $s = 0.12$; ♦, 80 wt %, $s = 0.28$; ●, 99 wt %, $s = 0.54$.

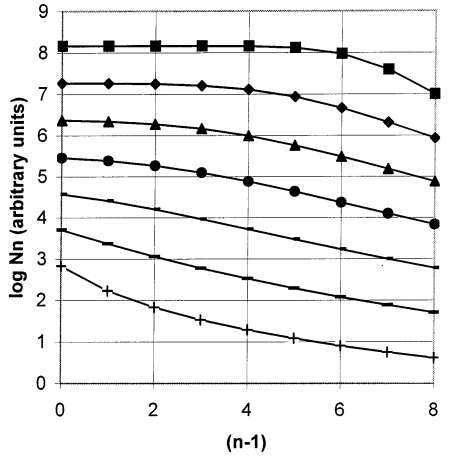

Figure 7. Simulated distributions of products (N_n) in the vapor from RS of P(19) at >99.9wt % loss as a function of DP(n) for $k_{evap} = 0$ for $n = 10-18$; $k_{evap} = 1$ for $n = 9$; and, in ascending order, $k_{evap} = 1$, 3.16, 10, 31.6, 1×10^2, 1×10^3, and 1×10^6 for $n = 1$; for gradation of k_{evap} between $n = 1$ and 9, see text: +, r^2 (forced linear least squares) = 0.941; −, $r^2 = 0.989$, $s = 0.44$; −, $r^2 = 0.998$, $s = 0.41$; ●, $r^2 = 0.974$, $s = 0.38$; ▲, $r^2 = 0.931$; ♦, $r^2 = 0.829$; ■, $r^2 = 0.599$. Ordinates offset by 1 log unit for clarity.

coupled cleavage and evaporation in open systems typically assume a critical L_c for "instantaneous" evaporation,[30a,35a,b,36] the expected N_c distribution for the volatiles is seldom, if ever, explicitly addressed. We now show by a simple scaling simulation that the value of s derived from the volatile products, as is the usual practice, is not a simple function of reaction progress but is influenced by the volatilization process.[86b]

We carried out numerical simulations[151] of idealized RS of a monodisperse model "polymer" limited for computational convenience in this scaling exercise to DP = 19. The polymer, P(19), and each of its cleavage products, P(2)−P(18), were allowed to undergo cleavages of the type P(n) → P(j) + P($n-j$) with $j = 1$ to $(n - 1)$. Each of these $\sum_2{}^{19}(n - 1) = 171$ cleavage events was assigned an identical formal first-order rate constant, $k_{scis} = 1$,[152] as assumed, for example, by Simha and Wall[36] and by Staggs.[35a] Evaporation steps P(n) → P(n)V were included up to an arbitrary limit of $n \leq 9$, where P(n)V has evaporated from the reaction zone and is thus protected from further cleavage; these steps were assigned a formal first-order rate constant, k_{evap}. Simulations for a closed system (all $k_{evap} = 0$) gave the expected conformance to the log $N_n \propto (n - 1)$ relationship as illustrated in Figure 5 for t values sufficient to convert 10, 40, 80, and 99 wt % of the P(19) fed to products with $n \leq 9$ ($t = 0.0212$, 0.0922, 0.254, and 0.637, respectively).[153−155] The progressively more negative slopes correspond to increasing formal s values of 0.03, 0.12, 0.27, and 0.52, respectively.[156] To mimic a parallel open system with $L_n = 9$, the simulations were repeated with k_{evap} set at an arbitrarily high value of 1×10^6 for $n \leq 9$ but 0 for $n \geq 10$. Had the melt been sampled at the same t values for P(10)−P(19) (not the usual practice), the rate of disappearance of P(19) and the P(10)−P(18) vs t profiles would have been found unchanged, since each of these products continues to be formed from larger species in the reaction zone and its disappearance rate is also unchanged. The formal s values from plots for $n = 10-18$ (solid lines in Figure 6) were virtually indistinguishable from those in Figure 5. Meanwhile, the amounts of P(1)−P(9) in the melt would have been found to be minuscule because of their "instantaneous" evaporation. On the other hand, had the escaped volatiles been analyzed for P(1)−P(9) (the usual practice), identical molar amounts of each species would have been found; i.e., the plots for $n = 1-9$ have $m = s = 0$ for *all* t (superimposed dashed lines in Figure 6). This counterintuitive behavior results because the formation rate of each P(n) with $n \leq 9$ is identical, i.e., d[P(n)]/dt = $2k_{scis}\sum_{10}{}^{19}$[P($n$)], and any further cleavage has been eliminated. Such a result is clearly at odds with all experimental data and removes any physical significance from the s value.

A more realistic situation would have k_{evap} increase as n decreases. A series of simulations were run with k_{evap} increased from an arbitrary constant value of 1 for P(9) ($^1/_8$ of its total k_{scis}) to a varied k_{max} for P(1). The dependence of k_{evap} on n for the intervening P(2)−P(8) must be complex. For this scaling exercise, we estimated log $k_{evap}(n) = (1.301 - 0.301n^{2/3})$ log k_{max}, following evidence that T_b and ΔH_v for n-alkanes scale as $n^{2/3}$.[83,157,158] Plots for the volatiles only are shown in Figure 7 for exhaustive pyrolysis (99.9^+ wt % loss) with k_{max} systematically increased from the unrealistically

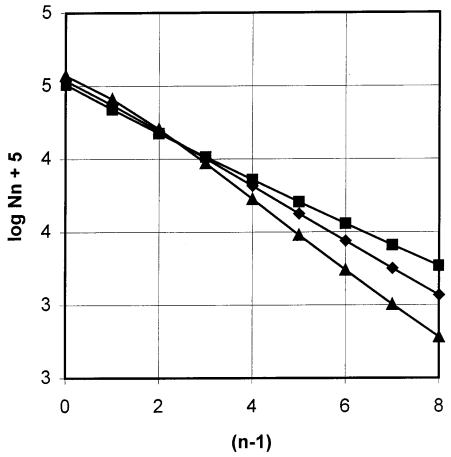

Figure 8. Simulated distributions of products (N_n) in the vapor from RS of P(19) as a function of DP(n) with $k_{evap} = 0$ for $n = 10-18$; $k_{evap} = 1$ for $n = 9$; and $k_{evap} = 10$ for $n = 1$; for gradation of k_{evap} between $n = 1$ and 9, see text: ■, 10 wt % loss, $s = 0.30$; ♦, 40 wt % loss, $s = 0.35$; ▲, >99.9 wt % loss, $s = 0.41$.

low extreme of 1 to the probably unrealistically high extreme of 1×10^6, specifically $k_{max} = 10^y$ with $y = 0$, 0.5, 1, 1.5, 2, 3, and 6. The plots were no longer linear but changed systematically from concave upward to concave downward as k_{max} increased. The nearest approach to linearity, as judged by the r^2 values of least-squares fits (see Figure 7), occurred for $k_{max} \approx 3-30$. Parallel plots (not shown) for 40 and 10 wt % loss showed subtle differences, but the same pattern of only a limited, albeit somewhat broader, region of "linearity" persisted. Plots as a function of wt % loss (10, 40, and >99.9%) for the specific case of $k_{max} = 10$ are shown in Figure 8. Whereas such plots of experimental data could easily be interpreted as "linear" within typical scatter, the formal values of s derived from least-squares plots were confined to the narrow range 0.30−0.41 for the wide range of t (0.140, 0.330, and 4.00) and wt % loss involved, compared with the much larger changes in s shown in Figure 5 for a closed system. Thus, the s parameter derived for open systems must be a complex function of both the rate of reaction and the relative rates of product evaporation and can no longer be interpreted simply as a probability of bond scission. Inversely, the empirically observed near-linear log N_c-c plots for PE pyrolysis (Figures 2 and 3) must set significant constraints on the dependence of evaporation rate on c to allow the perceived "linearity".

Backbiting. The nonstatistical local maxima and minima shown in Figures 2 and 3, along with similar but sometimes less complete patterns in other studies,[6a,9,30b,33c,58,67b,68,75,86a,87] led to proposals of superposition of BB on a RS background. Van Schooten and Evenhuis[57] rationalized maxima at $c = 3$, 6, 7, 10, and 11 and minima at $c = 5$, 8, and 9 in the in-line hydrogenated products from flash pyrolyses of both HDPE and LDPE at ≈500 °C by 1,5-shifts. Serial occurrence of step 4a with $x = 5$, followed by step 4b, would lead to ENEs at $c = 6$, 10, 14, ..., while competitive step 4c would lead to ANEs at $c = 3$, 7, 11, ... Tsuchiya and Sumi[63] also attributed favored production of ENEs at $c = 6$ and 10 and ANEs at $c = 3$, 7, and 11 from partial conversions of HDPE, LDPE, and PM at 375−437 °C to serial 1,5-shifts. They suggested that the second shift would be slower than the first, i.e., $k_{1,5}$(s,s) < $k_{1,5}$(p,s). Kiran and Gillham[72] perceived ENE maxima as high as $c = 18$ and ANE maxima as high as $c = 15$, suggestive of four successive 1,5-shifts, in products from LDPE heated to 600 °C at 20 °C/min.[159]

For exclusive 1,5-shifts, the local distributions around the predicted maxima at $c = 6$, 10, 14, ... for ENEs and $c = 3$, 7, 11, ... for ANEs should show $N_{c-1} > N_{c+1}$ from the underlying RS contribution. There is evidence, although not totally consistent,[64] for inversions of this inequality, e.g., ENE9 < ENE11[30b,63b,67a,72,87] and ANE10 < ANE12.[63b,72b,86a,87] These might indicate the competitive occurrence of 1,x-shifts with $x \neq 5$, specifically with $k_{16} > k_{14}$ (see below), and non-1,5 shifts have indeed been considered. Van Schooten and Evenhuis[57] were hesitant to propose 1,6-shift as a unique source of product at $c = 4$ because they expected $k_{1,5} \gg k_{1,6}$ (see below). Bailey and Liotta[56] proposed the 1,4-shift as a potential source of ethane and 1-pentene. Seeger and Cantow[86a] appear to have assumed that maxima in the in-line hydrogenated products at $c = 7$ and 11 as well as at $c = 6$ and 10 arose *only* from ENEs from step 4b and therefore deduced the presence of "excess" radical centers at C_6 and C_{10} as well as C_5 and C_9. To achieve the former, they proposed a (very unlikely) initial 1,2-shift followed by 1,5-shifts. In fact, the maxima at $c = 7$ and 11 more likely arose from ANEs derived from step 4c for radical centers at C_9 and C_{13}. The model of Faravelli and co-workers[30b] (see above and below) includes 1,4-, 1,5-, and 1,6-shifts.

Unzipping. Since the minimal yield of ethylene (Figure 1) falls near the extrapolated RS correlation lines (Figures 2 and 3), the UZ pathway (step 2) must be trivial. Seeger and Cantow[86a] proposed that this results from the strength of the C−C bonds in PE and the large quantity of hydrogens available for transfer (even though they are all *sec* rather than *tert*), while Wall[160] implied that the relatively unstable $R_p^\bullet$ has a characteristically low k_2/k_{3a} ratio (for no given reason). The significant yields of ethylene achieved under forcing conditions at high T in, for example, fluidized beds (see above) must represent "late" product from multiple repetitions of the RS pathway.[161]

Enlargement. The common mechanism proposed for MW increases in the lowest T range and the simultaneous and presumably causative formation of new LCBs is the combination of $R_s^\bullet$ and $R_p^\bullet$ (or of $R_s^\bullet$ with itself) (steps 6c or 6f),[46b,47,49] despite evidence for a long KCL (see above). An observation of Witt and Hogan[54] may suggest otherwise: the increase in MW of HDPE held at 190 °C was eliminated by hydrogenation of its TV groups but more surprisingly also by isomerization of those double bonds to internal positions. The latter structural change should, if anything, accelerate initiation by allylic-bond homolysis and thus not suppress a radical combination route to LCBs. An alternate mechanism that should however respond negatively would be radical addition of $R_s^\bullet$ (or $R_p^\bullet$) to TV groups in the initial and/or degrading polymer. The occurrence of such radical additions, essentially the reverse of steps 3a and 3b, is well documented during the pyrolysis of *n*-alkanes under low-T dense-phase conditions where the entropic driving force for cracking has not yet become overwhelming,[162] and they are known to be more rapid for terminal than for internal double bonds.[163]

To rationalize formation of LCBs and $f_t < 1$ (see above), Kuroki and co-workers[47a] dismissed radical combination, because of proposed serious diffusional restrictions, and proposed instead an unusual sequence

of (a) allylic end-group homolysis to form $R_p^\bullet$ and allyl radical, (b) hydrogen abstraction from polymer in the cage wall by allyl to form $R_s^\bullet$, and (c) intracage combination of the resulting ($R_p^\bullet$ + $R_s^\bullet$) pair. This sequence would require that allyl radical rather than $R_p^\bullet$ dominate the purported intracage transfer reaction; the authors acknowledged that estimated E_H values predict the reverse order and therefore made the further (unsatisfying) postulate that transfer within the cage would be controlled by diffusion rather than activation energy. In any case, it is not apparent how this mechanism produces the H-balance discrepancy ($f_t < 1$) since the only volatile produced, propylene, is neither H-poor nor H-rich.

Double Bond Formation. Propagation steps 3b, 4b, and 4c are obvious sources of TV functionality in the degrading polymer and of ENEs in the volatile products. However, no fully satisfying mechanism exists to rationalize the nonnegligible formation of VL and VD functionality under long-chain conditions (see refs 42 and 164 and the discussion in Supporting Information).

Computational Model for Initial Product Distributions

Model Structure and Approach. We estimate *initial* product distributions as a function of *c* at infinitesimal conversion based on estimated propagation rate constants, with particular emphasis on the BB and UZ pathways. Consider P1R ($R_p^\bullet$) formed in step 1 or 3b. ["P*m*R" indicates a polymer radical with the radical center at the *m*th carbon from the end; "*m*" is specified numerically for near-end radicals formed by 1,*x*-shifts but generically as "*n*" for random radicals formed by transfer; in general, $n \gg m$.] It has three competitive fates. (1) Transfer with P forms P*n*R and a polymer fragment with a saturated chain end, PANE1. [The suffix in PANE*m* indicates that it was formed from P*m*R.] Ultimate[99] β-scission of P*n*R forms a polymer fragment with an unsaturated chain end, PENE*n* [the suffix in PENE*n* indicates that it was formed from P*n*R], and regenerates P1R. Except for differences in DP of the initial and the regenerated P1R, the sum of these steps is one RS event of the backbone:

$$\text{P1R} + \text{P} \xrightarrow{k_H} \text{PANE1} + \text{P}n\text{R}$$

$$\text{P}n\text{R} \xrightarrow{k_\beta} \text{PENE}n + \text{P1R}$$

$$\sum\text{: P} \rightarrow \text{PANE1} + \text{PENE}n$$

(2) Competitive β-scission of P1R forms ethylene, ENE2 ["ENE*r*" indicates a 1-alkene with *r* carbons], and again regenerates P1R. This is the UZ event:

$$\text{P1R} \xrightarrow{k_\beta} \text{ENE2} + \text{P1R}$$

(3) 1,*x*-Shifts in P1R form isomeric P*m*R (*x* was limited to 4−6 in the present model). To close this cycle and regenerate P1R, each P*m*R has the same three fates as P1R. Further 1,*x*-shifts, in either direction along the chain, simply change the positional index "*m*". Serial 1,*x*-shifts can in principle eventually generate all positional isomers of P*m*R so long as *x* is not limited to only 5. Transfer of P*m*R produces an RS event for which the intervening 1,*x*-shift(s) is invisible except for the "bookkeeping" suffix on PANE*m*:

$$\text{P1R} \xrightarrow{k_{1x}} \text{P}m\text{R}$$

$$\text{P}m\text{R} + \text{P} \xrightarrow{k_H} \text{PANE}m + \text{P}n\text{R}$$

$$\text{P}n\text{R} \xrightarrow{k_\beta} \text{PENE}n + \text{P1R}$$

$$\sum\text{: P} \rightarrow \text{PANE}m + \text{PENE}n$$

β-Scission of P*m*R toward the chain interior forms ENE(*m*+1) and regenerates P1R. The net result is excision of ENE(*m*+1):

$$\text{P1R} \xrightarrow{k_{1x}} \text{P}m\text{R}$$

$$\text{P}m\text{R} \xrightarrow{k_\beta} \text{ENE}(m+1) + \text{P1R}$$

$$\sum\text{: P1R} \rightarrow \text{ENE}(m+1) + \text{P1R}$$

β-Scission of PmR toward the chain end forms PENE*m* and a small alkyl radical Ar*s*R. ["Ar*s*R" indicates a linear alkyl radical with *r* carbons and the radical on the *s*th carbon; for the initial β-scission, $s = 1$.] If Ar1R undergoes transfer to form ANE*r* ["ANE*r*" indicates a *n*-alkane with *r* carbons], the cycle back to P1R is closed as follows:

$$\text{P1R} \xrightarrow{k_{1x}} \text{P}m\text{R}$$

$$\text{P}m\text{R} \xrightarrow{k_\beta} \text{PENE}m + \text{Ar1R} \qquad r = m - 2$$

$$\text{Ar1R} + \text{P} \xrightarrow{k_H} \text{ANE}r + \text{P}n\text{R}$$

$$\text{P}n\text{R} \xrightarrow{k_\beta} \text{PENE}n + \text{P1R}$$

$$\sum\text{: P} \rightarrow \text{PENE}m + \text{ANE}r + \text{PENE}n \qquad r = m - 2$$

As noted above, RS and BB are stoichiometrically coupled by this latter process in which PANE*m* is replaced as product by PENE*m* and ANE*r*. Thus, in principle, both exclusive RS and exclusive UZ are possible, but BB must always be accompanied by ≈50% RS. Finally, since Ar1R can undergo not only transfer but also its own 1,*x*-shifts and β-scissions, we include all its fates in analogous fashion until some Ar*s*R finally undergoes transfer to close the path back to P1R. Serial 1,*x*-shifts can generate almost all the *sec* radical positional isomers of Ar*s*R:[165]

$$\text{Ar}s\text{R} \xrightarrow{k_{1x}} \text{Ar}(s+3)\text{R} + \text{Ar}(s+4)\text{R} + \text{Ar}(s+5)\text{R} + \text{Ar}(s-3)\text{R} + \text{Ar}(s-4)\text{R} + \text{Ar}(s-5)\text{R}$$

Their β-scissions provide additional sources of ENE*r* along with still smaller Ar1R:

$$\text{Ar}s\text{R} \xrightarrow{k_\beta} \text{ENE}(s+1) + \text{A}(r-s-1)\text{1R}$$

$$\text{Ar}s\text{R} \xrightarrow{k_\beta} \text{ENE}(r-s+2) + \text{A}(s-2)\text{1R}$$

Eighteen generic rate constants are required to describe these cycles of reactions that originate and end with P1R: (1) transfer with P via k_H(p,s) and k_H(s,s) [the first index, p = *prim* or s = *sec*, is the attacking radical and the second is the radical formed]; (2)

β-scission to expel either a *prim* or methyl radical via k_β(p,p), k_β(s,p), k_β(p,Me), and k_β(s,Me) [the first index is the cleaving radical and the second is the radical expelled]; and (3) 1,4-, 1,5-, and 1,6-hydrogen shifts via k_{14}(p,p), k_{14}(p,s), k_{14}(s,p), k_{14}(s,s), k_{15}(p,p), k_{15}(p,s), k_{15}(s,p), k_{15}(s,s), k_{16}(p,p), k_{16}(p,s), k_{16}(s,p), and k_{16}(s,s) [the first index is the attacking radical and the second is the radical formed; in the literature, these indices are sometimes reversed]. For each intermediate radical to which z decay steps each are available, we define the fraction consumed by a given step as $f_z = k_z/\sum k_z$. For β-scission or 1,x-shift, "k_z" is the first-order rate constant k_β or $g_{1x}k_{1x}$, where g_{1x} is the reaction path degeneracy, either 2 or 3. For transfer, it is the pseudo-first-order rate constant $g_H k_H[M] = g_H k_H \rho/m_0$, where $g_H = 4$. Having estimated these rate constants, one could in principle obtain the initial distributions of the volatiles ENEr and ANEr as a function of r and of the new end groups PANE $= \sum$PANEm and PENE $= \sum$PENEn + $\sum$PENEm by constructing a series of nested fractions based on the f_z values. However, the algebra quickly becomes convoluted, especially because a given PmR can sometimes be regenerated after a series of 1,x-shifts.

Rather we chose a Monte Carlo type approach. A cycle begins with P1R and ends when P1R is ultimately regenerated, along with the appropriate initial product(s). Since our focus is on the *initial products and functionalities* formed rather than the DP of the residual polymer, no attempt was made to distinguish that the regenerated P1R will have a DP different from the initial one "injected" to start a cycle. For each radical encountered during a cycle, an interval between 0 and 1 is partitioned into its decay fractions f_z. This unit interval thus has $(z - 1)$ dividing markers: $F(1) = k_1/\sum k_z$, $F(2) = (k_1 + k_2)/\sum k_z$, ..., $F(z - 1) = (k_1 + ... + k_{z-1})/\sum k_z$. A random number between 0 and 1 is generated, whose value will fall into one of the z intervals $0-F(1)$, $F(1)-F(2)$, ..., $F(z - 1)-1$ and will thus specify which of the z possible decay steps will occur for that radical in that cycle. The stable product from that step is tallied. The partitioning process with a newly generated random number is repeated for the new radical produced. All products formed from a large number of cycles are summed until their relative amounts become essentially independent of the number of cycles (1×10^6 cycles usually sufficed), at which point the relative probabilities for their initial formation have been established, based on the rate constants assigned. Because of the statistical nature of the approach which considers all decay steps available to each radical, identity reactions, which can occur for certain of the 1,x-shifts in Arsr, are included. For the PmR radicals formed by serial 1,x-shifts toward the chain interior, the set was truncated at $m = 30$ for practical computational reasons. Thus, a small, but known and usually trivial, fraction of PmR even further into the chain interior were "discarded".

To visualize the procedure, the shortest route from P1R back to P1R forms ENE2 by UZ; this ethylene was labeled as "ENE2Z" to distinguish it from ENE2 formed from Ar1R species. The two-step RS route forms PANE1 and PENEn by transfer and β-scission of PnR. More extended routes involving 1,x-shifts sample numerous radicals before P1R is regenerated and produce varying fractions of PANEm, PENEm, ANEr, and/or ENEr. The ENEr formed specifically from β-scission of PmR radicals, which is labeled "ENErBB", is somewhat smaller than and is counted separately from the total ENEr that includes some ENEs formed from Arsr. By material balance for transfer, $(\sum$PANE$m + \sum$ANE$r) = \sum$PnR $= \sum$PENEn; by material balance for β-scission of PmR toward the chain end, $\sum$PENE$m = \sum$ANEr.

Table 4. Rate Constants Used for Modeling Initial Product Distributions

	base set[a]			F−R set[a,b]		
process	log A	E	log k_{773}	log A	E	log k_{773}
k_H(p,s)[c]	8.28	12.8	4.66	8.00	11.2	4.83
k_H(s,s)[c]	8.11	14.2	4.10	8.00	12.2	4.55
k_β(p,Me)	12.76	30.1	4.26	14.00	32.0	4.95
k_β(p,p)	13.03	27.8	5.16	14.00	30.0	5.52
k_β(s,Me)	14.04	32.8	4.78	14.00	33.0	4.67
k_β(s,p)	14.48	31.7	5.51	14.00	31.0	5.23
k_{14}(p,p)[c]	11.00	22.0	4.78	11.00	20.6	5.18
k_{14}(p,s)[c]	11.20	20.8	5.31	11.00	18.3	5.83
k_{14}(s,p)[c]	10.91	23.7	4.21	11.00	21.6	4.89
k_{14}(s,s)[c]	11.00	22.2	4.73	11.00	19.3	5.54
k_{15}(p,p)[c]	10.10	15.0	5.85	10.20	14.5	6.10
k_{15}(p,s)[c]	10.26	13.7	6.38	10.20	12.2	6.75
k_{15}(s,p)[c]	9.97	16.6	5.28	10.20	15.5	5.82
k_{15}(s,s)[c]	10.10	15.2	5.81	10.20	13.2	6.47
k_{16}(p,p)[c]	9.86	15.6	5.45	9.70	14.5	5.60
k_{16}(p,s)[c]	10.02	14.3	5.98	9.70	12.2	6.25
k_{16}(s,p)[c]	9.73	17.2	4.88	9.70	15.5	5.32
k_{16}(s,s)[c]	9.86	15.8	5.40	9.70	13.2	5.97

[a] Units are M, s, and kcal mol^{-1} as appropriate; see details in Tables S5−S7. [b] Reference 30. [c] Per H.

Selection of Rate Constants for Model. The database on thermochemistry and rate constants for small radicals in the gas phase is much expanded over that available to Mita[1d] 25 years ago. Estimates for the 18 required rate constants in Arrhenius form are given in Table 4 and rely heavily on the NIST kinetic database,[121e] thermochemical balance, and internal consistency within each reaction class. Details of the estimation processes used are given in the Supporting Information, including Tables S5-S7; a brief sketch is given here.

Estimates for k_H are based on the recommendations by Tsang[121a,121b] for small species at 300−2500 K. Values of log A_H (per H), E_H, and $k_{H,773}^{rel}$ are collected in Table S5.[166,167] The modest inequality E_H(s,s) < E_H(p,p) for the thermoneutral cases is consistent with recently proposed trends.[168]

Values for three of the required k_β values are available from the Slagle−Gutman group, based on recent experimental measurements, thermochemical balance, and evaluations of earlier data; these are listed in Table S6. The value chosen for k_β(p,Me) was for *n*-propyl,[169a] the exact example involved in PE pyrolysis;[170] that for k_β(p,p) was for *n*-butyl;[169b] and that for k_β(s,Me) was the average of two nearly identical values for *sec*-butyl.[169d,171] Since there is no radical in these studies to serve as the prototype for k_β(s,p), we started with a recent estimate by Yamauchi and co-workers[172] based on kinetic studies and TST calculations for an average for 2-pentyl, 2-hexyl, and 3-hexyl. Two earlier values derived from mechanistic analyses of complex reaction systems span this estimate with a spread of 6-fold.[173] However, pattern analysis of the Slagle−Gutman data, along with evidence on the behavior of 3-hexyl during the pyrolysis of *n*-hexane,[174,176] caused us to increase the Yamauchi value a factor of 2 (Table S6). Although the ratios k_β(s,Me)/k_β(p,Me) = 3.3 and k_β(s,p)/k_β(p,p) = 2.2 at 773 K may appear counterintuitive, they conform to a known pattern[104b] that the more stable radical is indeed the

more reactive, presumably indicative of a compensating role of the additional alkyl substituent in stabilizing the olefin formed.[1d]

The anchoring value for 1,4-shift was k_{14}(p,s) (Table S7) taken from recent analyses of new and previous data for 1-pentyl at 350−1300 K by Yamauchi and co-workers.[172] It overlaps well with earlier data at both the low-T[177] and high-T[178] ends of the range. The remaining values for the 1,4-shift (Table S7) were assigned by thermochemical balance and assumption of the same selectivities as for transfer.[179] A corresponding recommendation of Yamauchi and co-workers[172] was used for k_{15}(p,s) in 1-hexyl at 350−1300 K.[181] It overlaps well with earlier data at the low-T end[180,182] but gives values 2−3-fold greater in the 673−873 K regime than would be extrapolated from those low-T expressions. Thermochemical balance and selectivities for transfer were again used to complete Table S7 for 1,5-shifts. Extrapolating an experimental value of k_{15}(s,s) for 3-octyl → 2-octyl at much lower T (300−385 K)[180] gives excellent agreement.[183]

Kinetic data for 1,6-shift is scarce, and different models lead to conflicting results for the relative magnitude of k_{16} and k_{14}. Focusing on the strain energy and the entropy constraints to achieve the cyclic transition state for the 1,x-shift, Benson[103a] predicted $k_{16} < k_{14} < k_{15}$. Dobe and co-workers[180] used a similar model and predicted $E_{16} \approx E_{14}$ (the strain energies of cyclopentane and cycloheptane are each ≈6 kcal mol^{-1} relative to cyclohexane[185]) but $A_{16}/A_{14} \approx 10^{-2}$ because of the need to freeze out two additional C−C rotors, i.e., k_{16}:$k_{14} \approx$ 1:100. From another similar model, Lehrle and Pattenden[186] predicted k_{16}:k_{15}:$k_{14} \approx$ 1:100:5 at 623 K, i.e., the same inequality of $k_{16} < k_{14}$ but on a more compressed scale. However, other evidence supports the reverse inequality $k_{16} > k_{14}$. Larson and co-workers[187] found k_{14}:k_{15}:k_{16} = 1:100:5 for (s,s) shifts in chemically activated 2-nonyl radical, exactly the reverse of the Lehrle−Pattenden model.[186] An early hypothesis of 1,x-shifts was made to rationalize the formation of SCBs in LDPE during free-radical polymerization.[5] Although there is considerable scatter in data on SCB distributions, the trend is clearly butyl > pentyl ≈ (hexyl + higher) ≫ propyl,[2,59,60,188,189] also in accord with the reverse inequality $k_{15} > k_{16} > k_{17} \gg k_{14}$. Mattice and Stehling[188d] applied a rotational isomeric state model to P1R and estimated $k_{15} \gg k_{16} \geq k_{17} > k_{18} \approx k_{14}$.[190] Viskolcz and co-workers[191] estimated k_{16}:k_{15}:k_{14} of 1.6:1.0:0.02 at 773 K for 2-methyl-1-hexyl, 1-pentyl, and 1-butyl from ab initio calculations. In light of this admittedly conflicting evidence, we chose to base the ratio of k_{16}(p,s):k_{15}(p,s) on the ratio of butyl:pentyl SCBs in LDPE, which appears to be ≈3 at a polymer synthesis $T \approx$ 523 K,[188] and arbitrarily split this small difference between A and E (Table S7). Thermochemical balance and selectivities for transfer were again used to complete Table S7 for 1,6-shifts. These estimates give k_{16}:k_{15}:k_{14} = 27:68:6 at 773 K.[192,193]

The term $g_H k_H \rho/m_0$ requires an expression for $\rho(T)$ for molten PE. Available data (ρ in g/mL and T in °C) are all at T below that for active decomposition and a rather long extrapolation is needed. We chose the expression $(1/\rho) = 1.142 \exp(7.7 \times 10^{-4} T)$ based on our various fits to self-consistent reported data;[194,195] other reports[196,197] would give somewhat different correlations.

Possible Polymer-Specific Effects on Rate Constants. We assume herein, as did Faravelli and Ranzi (F−R),[30] that these estimates for the propagation rate constants derived from small-molecule behavior, largely in the gas phase, can be transferred to the polymer melt conditions. Evidence for this simplification[40f] and the "principle of equal reactivity"[198] is significant although not overwhelming. In a review of diffusion control in reactions of small molecules and radicals with polymers, Mita and Horie[1f] gave examples in which the rate constant k_H for very rapid hydrogen abstraction from polymers in solution (e.g., by hydroxyl radical), calculated from the rate expressed as k_H[M], decreased with increasing MW. This phenomenon was attributed to reaction at almost every collision of the radical with the "surface" of the (widely separated) polymer coils; in other words, most of the reactive hydrogens within the polymer coil were never sampled, and it would be more appropriate to express the rate as k_H[P]. However, relevant to consideration of melts, these MW effects disappeared at high concentration, and it was concluded that "at high concentrations where polymer molecules overlap or interpenetrate, the concentration can be approximated as a uniform solution of monomer units and the value of k in units M^{-1} s^{-1} is independent of ... [DP]." Effects of MW were also predicted to disappear for reactions for which the rate-determining step involves a significant chemical activation energy, as does transfer, rather than diffusion.[199,200] In contrast, in their recent mechanistic model for pyrolysis of polystyrene, Broadbelt and co-workers[41a] chose to scale k_H values as the inverse of the DP of the attacking radical, following an analysis of hexadecane cracking data and collision-theory arguments offered by Watanabe and co-workers.[202]

There is growing evidence that k_{add} for the first propagation step in solution free-radical vinyl polymerization (which would be in effect a small model system) is 10−50-fold greater than the normally measured propagation rate constant, k_p, for formation of high polymer.[203] Fischer and Radom[163] summarized the evidence and observed that the diminution in k_{add} as the size of the adding radical increases reflects largely an order of magnitude decrease in A, coupled with a more modest increase in E. They therefore suggested an increasing loss in conformational freedom to achieve the transition state as the size of the attacking radical increases. Since such entropic factors should affect the equilibrium constant K_{add} in fashion similar to k_{add}, the effect of radical size on the reverse k_β ($\equiv k_{add}/K_{add}$) would be expected to be much smaller.

With respect to possible "polymeric effects" on k_{1x}, Wall and Strauss[143] speculated that the greater branching in LDPE compared with HDPE would favor BB over transfer by inhibiting the latter, because they pictured branched LDPE as "more spherical" with the least reactive side-chain methyl groups of the branches on the outside and the most reactive *tert* hydrogens buried; they also considered that steric effects would disfavor transfer as the attacking radical became more bulky. Ranzi and workers[30a,202] initially suggested that BB would be inhibited in the liquid compared with the gas phase because of resistance to internal rotations of large C−C segments and would therefore occur largely at the interface between the degrading melt and bubbles of sweep gas and/or evolving gaseous products; however, they did include BB generally in a later model[30b] (see above). Murata and co-workers[19] made a similar assertion with no further justification. Conversely, McCaffrey

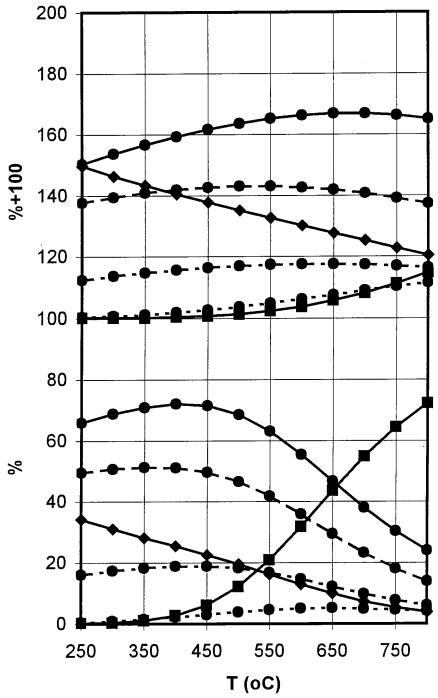

Figure 9. Distribution of initial decay processes available to P1R (upper portion) and P*m*R or P*n*R (lower portion) in the kinetic model as a function of *T*: ■, *β*-scission; ♦, transfer; ●, 1,*x*-shift. For the latter, solid line, total 1,*x*-shift; long dashed line, 1,5-shift; alternating dashed line, 1,6-shift; short dashed line, 1,4-shift.

and co-workers[13b] speculated that serial 1,5 shifts would be favored compared with small-molecule models because the coil configuration of the polymer would align the carbons favorably for serial transfer. We are not aware of any attempt to apply chain-end dynamic simulations to this problem as N_e traversed.

General Model Output. Simulations with the rate constants in Table 4 were carried out over the range 250−800 °C. The stoichiometric definitions of the three pathways follows: (1) RS following transfer is identified with ∑PENE*n* from the first backbone cleavage;[205] (2) UZ is identified with ENE2Z; and (3) *effective* BB, i.e., 1,*x*-shift(s) followed by *β*-scission rather than transfer or further 1,*x*-shifts, is divided into two classes, that toward the chain interior identified with ∑ENE*r*BB and that toward the chain end identified with ∑PENE*m*.[206] The latter pathway also forms some "xsENE*r*" ≡ (∑ENE*r* − ∑ENE*r*BB − ENE2Z), i.e., those ENEs derived not from *β*-scission of polymer radicals but of ArsR species before they ultimately form still smaller ANEs by transfer. Note that production of volatile ANEs without DIENEs from BB does not violate the stoichiometric constraints discussed above because the "excess H" is balanced by formation of more unsaturated than saturated end groups in the residual polymer (∑PENE*n* > ∑PANE*m*) compared with the ideal 1:1 ratio expected from RS alone.

The ratio of pathways available to P1R is 1,*x*-shift:transfer:unzipping = $\{2k_{14}(p,s) + 2k_{15}(p,s) + 2k_{16}(p,s)\}$:$4k_H(p,s)(1000\rho/28)$:$2k_\beta(p,p)$; this competition as a function of *T* is shown in the upper part of Figure 9. At the lowest *T*, the relative rate of unzipping is trivial while those of the 1,*x*-shift and transfer are essentially identical. As *T* increases, unzipping emerges to a detectable level largely at the expense of transfer while the 1,*x*-shift is the least affected; this pattern follows from the assigned

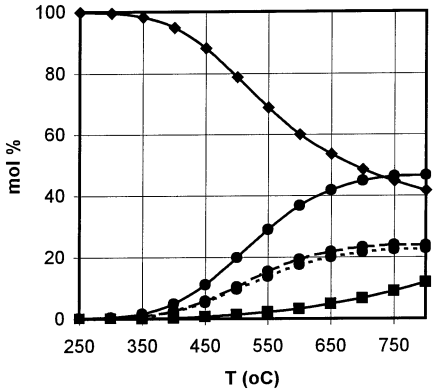

Figure 10. Distribution of initial product classes predicted by the kinetic model as a function of *T*: ■, UZ; ♦, RS of backbone; ●, effective BB. For latter, solid line, total BB; long dashed line, BB toward the interior of the chain; short dashed line, BB toward the end of the chain.

$E_\beta > E_{15} \geq E_H$. If P1R is converted to P*m*R by 1,*x*-shift(s) or to P*n*R by transfer, the analogous ratio of pathways available to an on-chain radical[207] is 1,*x*-shift:transfer:unzipping = $\{4k_{14}(s,s) + 4k_{15}(s,s) + 4k_{16}(s,s)\}$:$4k_H(s,s)(1000\rho/28)$:$2k_\beta(s,p)$. This competition, shown in the lower part of Figure 9, is similar except for a larger relative selectivity for *β*-scission that arises from the assignment $k_\beta(s,p) > k_\beta(p,p)$.

The predicted initial product distributions shown in Figure 10 are notably different; RS totally dominates at the lowest *T* and only at higher *T* do effective BB products emerge, along with the UZ product to an even lesser extent. The "disparity" between Figures 9 and 10 results because the kinetic barrier to effective BB at lower *T* lies more with *β*-scission of P*m*R than its formation by a 1,*x*-shift because of the higher *E* value of the former process. Thus, most of the 1,*x*-shifts at low *T* remain "invisible" because they culminate in transfer and RS rather than BB. As *T* increases, the number of xsENE*r* produced per A*rs*R formed increases from 0.00 to 0.27, a similar reflection of a steadily increasing fraction of *β*-scission of A*rs*R compared with transfer.

Simulated initial distributions of volatile ANEs, ENEs, and their sum at 400, 550, and 700 °C are shown in Figure 11 in the log N_c−*c* format. In the model these volatiles result *only* from BB (and, for most of ENE2, from UZ) but *not* from RS because only one backbone bond is allowed to break in the cycle from P1R back to P1R, and the successive backbone cleavages required to produce volatiles from RS are not addressed. The maxima expected for the predominant 1,5-shift can be seen at $c = 3, 7, \ldots$ for ANE*s* and at $c = 6, 10, \ldots$ for ENE*s*. However, the parallel, albeit less frequent, occurrence of 1,6- and 1,4-shifts leads to BB products at *every c*. The inequality $k_{16} > k_{14}$ leads to unsymmetrical broadening of the maxima toward the next higher *c* value, especially for the higher *c* values, e.g., ANE16 ≈ ANE15 and ENE15 ≈ ENE14. In the log(ANE + ENE) plot, as would be obtained experimentally in pyrolyses with an in-line hydrogenation step, the composite maxima are centered at $c = 6, 10, \ldots$ but broadened toward the next higher *c* value; this pattern results because ENE(*c*) is derived from P(*c*−1)R whereas ANE(*c*+1) is derived from the more internal and therefore less prevalent P(*c*+3)R. As an empirical parameter to characterize these distributions, we use the forced linear least-squares slope, *m′*, of the log N_c−*c* plot over the range $c = 3-20$; note that *m′* is a fundamentally

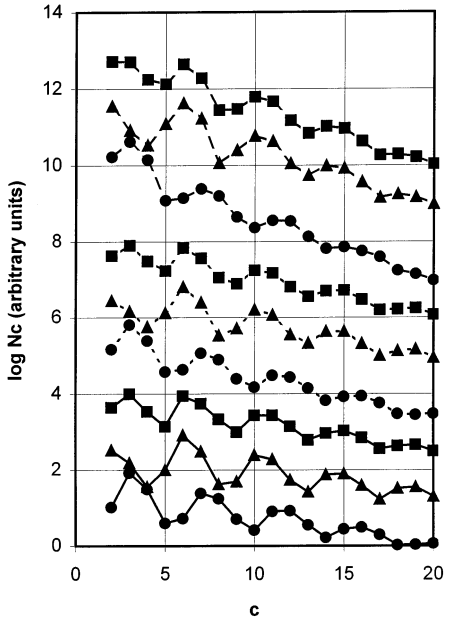

Figure 11. Distribution of volatiles (N_c) by carbon number (c) predicted by the kinetic model: ●, ANE; ▲, ENE; ■, (ANE + ENE). Solid lines, 400 °C; short dashed lines, 550 °C; long dashed lines, 700 °C. For each T, the log(ANE + ENE) plot and the log ENE plot are offset +2 and +1 units from the log ANE plot.

different quantity from the slope m derived from the high-c region of the experimental data in Figures 2 and 3 and used to characterize a RS distribution. Rather, m' characterizes the distance of the 1,x-shift into the chain and becomes less negative as this distance increases. The second parameter v over the range c = 3−20 is defined however the same as above and empirically characterizes the extent of alternation of log N_c between successive c values.[208] Increasing occurrence of 1,x-shifts up and down the chain compared with β-scission or transfer increasingly isomerizes the PmR family toward equilibrium, compared with the characteristic maxima resulting from k_{15} alone, and thereby reduces v. The m' values for log ANE, log ENE, and log(ANE + ENE) become increasingly more negative with increasing T; e.g., m' for log(ANE + ENE) changed from −0.075 to −0.099 to −0.154 over the T range shown. This decreasing average distance of the 1,x-shift into the chain before β-scission occurs follows from the inequality $E_\beta > E_{1x}$. In contrast to m', the v values were only modestly and not unidirectionally dependent on T, being in the range 0.33−0.39 for the ENEs, 0.24−0.29 for the ANEs, and 0.25−0.29 for the sum.

Sensitivity Analyses. The response of the model output to 10-fold decreases and increases in rate constants from the base set in Table 4 for the intermediate T = 500 °C[209] is shown in Table 5. A 100-fold increase in the k_H's about the median assignments increased the fraction of RS from slightly less than half to total dominance. For the corresponding steadily decreasing fraction of volatiles from BB/UZ, m' became more negative and v increased, indicating that increasing the probability of transfer shortened the average distance of the 1,x-shift into the chain and decreased the opportunities for isomerizations among PmR radicals before their β-scission. A 100-fold increase in the k_β's about the median assignments not only increased the fraction of UZ from trivial to modest but also, less intuitively, significantly increased the inherently larger fraction of BB, both at the expense of RS. The latter effect, which was even greater at lower T and persisted up to ≈650 °C, again highlights the kinetic barrier for effective BB at lower T as the β-scission step of PmR rather than the 1,x-shift that forms it. For this increasing BB fraction associated with increasing k_β, m' again became more negative and v increased, as it was now increased β-scission that shortened the average distance of the 1,x-shift into the chain and decreased the opportunities for isomerizations among PmR radicals. Finally, a 100-fold increase in the k_{1x}'s about the median assignments increased the fraction of BB, largely at the expense of RS. The dynamics of this effect can be conveniently visualized by considering its limits; were $k_{1x} = 0$, no BB products would be formed; as $k_{1x} \rightarrow \infty$, complete equilibration among the PmR isomers would be approached, and the fraction of BB would be $2k_\beta(\mathrm{s,p})/\{2k_\beta(\mathrm{s,p}) + 4k_H(\mathrm{s,s})(\rho/m_0)\} = 0.38$ at 500 °C for the base rate constant set. Simultaneously, the already minor fraction of UZ decreased even further. This indirect effect results because increasing the k_{1x}:k_β ratio increases the population of PmR radicals with $m > 1$ compared with P1R. In contrast with the effects of increasing k_H and k_β, increasing k_{1x} led to a less negative m' and a smaller v, since increasing k_{1x} lengthened the average distance of 1,x-shifts into the chain and led to more extensive equilibration among PmR isomers.[210]

In a second sensitivity exploration, the relative magnitudes of k_{14}, k_{15}, and k_{16} were changed while holding their sum, $\sum k_{1x}$, constant. In the base assignment (Table 4), k_{14}:k_{15}:k_{16} = 6:68:27 and k_{14}/k_{16} = 0.22 at 500 °C, essentially identical for the (p,p), (p,s), (s,p), and (s,s) categories. The m' and v values for three variants from this base assignment (case 1) are compared in Table 6: (1) an extreme case 2 in which all selectivity was removed (k_{14}:k_{15}:k_{16} = 33.3:33.3:33.3), (2) an opposite extreme case 3 in which the 1,5-shift was strongly dominant (k_{14}:k_{15}:k_{16} = 1:98:1), and (3) a case 4 in which the proportions of 1,4- and 1,6-shift were inverted (k_{14}:k_{15}:k_{16} = 27:68:6 and k_{14}/k_{16} = 4.6) toward the selectivity recommended by Lehrle and Pattenden.[186] The m' values, which are dependent mainly on $\sum k_{1x}$, are not significantly perturbed but major variations occur in v. The sharp and expected contrast in predicted c distributions for (ANE + ENE) is illustrated in Figure 12 for the least (case 2) and most selective (case 3) assignments[211] compared with the base assignments (case 1). The more subtle contrast between case 1 and case 4, for which the v values are similar, is also shown in Figure 12. Whereas for the assigned $k_{14} < k_{16}$ each log(ANE + ENE) maximum is unsymmetrically broadened toward the next higher c value ($N_{c+1} > N_{c-1}$) as noted above, for the inverted $k_{14} > k_{16}$ each maximum is broadened toward the next lower c value ($N_{c+1} < N_{c-1}$).

Formal Superposition of Volatiles from RS onto Model Output. Since our model of initial behavior does not produce volatiles from RS, we explored a hybrid approach to simulate the composition of the volatiles at realistic conversions in a closed system by mathematically combining varying proportions of the BB/UZ component from the model and the RS component from the relationship $N_c = C(1 - s)^{c-1}$. This approach assumes first that the BB/UZ component will continue to produce volatiles with the same initial c distribution as reaction proceeds toward completion. Although the contributory [M] term fortunately changes only mod-

Table 5. Sensitivity of Model Output to Rate Constant Assignments at 500 °C

rate constant class (multiple of base)[a]			product fraction			log N_c−c parameters	
k_H[b]	k_β[b]	k_{1x}[b]	RS	BB	UZ	m'	v
0.1	1	1	0.41	0.57	0.017	−0.077	0.19
1	*1*	*1*	*0.79*	*0.20*	*0.013*	*−0.088*	*0.24*
10	1	1	0.99	0.01	0.003	−0.18	0.44
1	0.1	1	0.97	0.03	0.001	−0.070	0.21
1	*1*	*1*	*0.79*	*0.20*	*0.013*	*−0.088*	*0.24*
1	10	1	0.52	0.38	0.099	−0.16	0.39
1	1	0.1	0.92	0.05	0.029	−0.22	0.41
1	*1*	*1*	*0.79*	*0.20*	*0.013*	*−0.088*	*0.24*
1	1	10	0.71	0.29	0.003	−0.044	0.086
Faravelli−Ranzi set[c]			0.92	0.07	0.016	−0.059	0.17

[a] Base rate constant set from Table 4 in italics. [b] Base rate constant normalized to unity for each class; variations tested are 10-fold less or 10-fold greater. [c] Reference 30.

Table 6. Sensitivity of Model Output to Relative Proportions of 1,*x*-Shift for Constant $\sum k_{1x}$ at 500 °C

	k_{rel}[a]			m'			v		
selectivity	k_{14}	k_{15}	k_{16}	ENE	ANE	ANE + ENE	ENE	ANE	ANE + ENE
case 1: base assignments[b]	5.7	67.8	26.5	−0.065	−0.102	−0.088	0.33	0.24	0.24
case 2: no selectivity	33.3	33.3	33.3	−0.082	−0.106	−0.094	0.15	0.12	0.10
case 3: high 1,5 selectivity	1	98	1	−0.074	−0.101	−0.096	0.82	0.78	0.71
case 4: inverted k_{14}:k_{16}	26.5	67.8	5.7	−0.082	−0.111	−0.098	0.27	0.21	0.23

[a] k_{1x} relative to $\sum k_{1x} = 100$ for each case. [b] Absolute values of k_{1x} in Table 4.

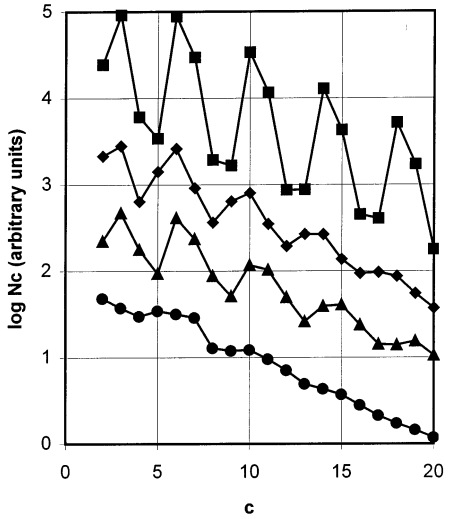

Figure 12. Distribution of volatile (ANE*s* + ENE*s*) (N_c) by carbon number (c) predicted by the kinetic model as a function of 1,*x*-shift selectivity (x = 4−6, see Table 6) at 500 °C: ■, case 3 (greatest 1,5 selectivity); ♦, case 4 (1,4 and 1,6 selectivities inverted); ▲, case 1 (base case); ●, case 2 (no selectivity). Ordinates offset by arbitrary amounts for clarity.

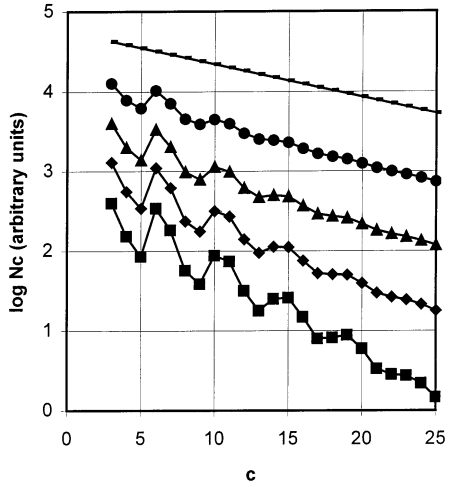

Figure 13. Distribution of volatile (ANE*s* + ENE*s*) (N_c) by carbon number (c) from superposition of BB products predicted by the kinetic model and RS products from a statistical distribution with s = 0.09 at 550 °C: ■, 0% RS (m = −0.103, v = 0.245); ♦, 25% RS (m = −0.066, v = 0.184); ▲, 50% RS (m = −0.053, v = 0.138); ●, 75% RS (m = −0.046, v = 0.090); −, 100% RS (m = −0.041, v = 0.041). Ordinates offset by arbitrary amounts for clarity.

estly with increasing x, this will be a gradually poorer approximation as x increases as additional pathways, such as those involving allylic sites, become more important and "late" reactions of initial products increase. Second, it assumes that the RS component will conform to linear log N_c−c behavior; thus, for comparison to data from the more common open systems, we make the further pragmatic assumption that linear log N_c−c behavior will remain a good *empirical* descriptor of RS products, based on experimental evidence such as in Figures 2 and 3, despite the fundamental complications from relative evaporation rates described above. Calculating such additive profiles requires assigning an s value for the RS contribution. The constant C can then be adjusted to control the fraction of RS products added. To conform to the usual experimental variable of weight loss, the fraction of RS added is expressed on the basis of wt %,[153] although the distribution plots are of course still shown in terms of N_c. The "wt % RS" values given below refer specifically to total products over the range c = 1−25. Figure 13 shows composite profiles for 0, 25, 50, 75, and 100 wt % RS for an intermediate T = 550 °C with an assigned s = 0.09 for RS, a value typical of experimental data (Table 2).[212] As nonstatistical BB is gradually replaced by statistical RS, m (not m') for the range c = 16−25 becomes decreasingly negative from −0.103 to −0.041, as the product distribution shifts toward higher c, and v for the range c = 3−20 decreases from 0.245 toward the limit of $v_{random} = |\log(1 - s)| =$ 0.041. Corresponding profiles as a function of T for a constant 50 wt % RS with an assumed s = 0.09 are shown in Figure 14; although the effects on m and v are smaller, the greater depth of BB into the chain at the lower T can still be seen. Finally, again for 50 wt % RS, the effect of variation in the assigned s parameter is shown in Figure 15. Increasing s leads to a more

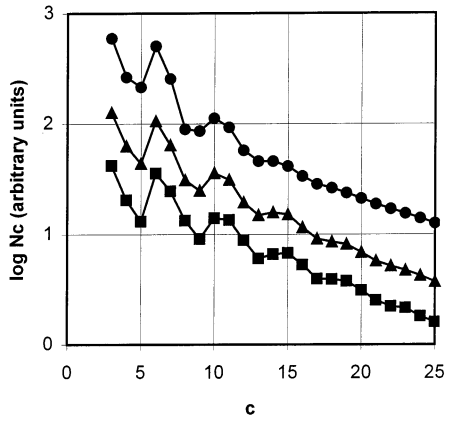

Figure 14. Distribution of volatile (ANE*s* + ENE*s*) (N_c), by carbon number (*c*) from superposition of 50% BB products predicted by the kinetic model and 50% RS products from a statistical distribution with $s = 0.09$: ■, 400 °C ($m = -0.055$, $v = 0.142$); ▲, 550 °C ($m = -0.053$, $v = 0.138$); ●, 700 °C ($m = -0.046$, $v = 0.138$). Ordinates offset by arbitrary amounts for clarity.

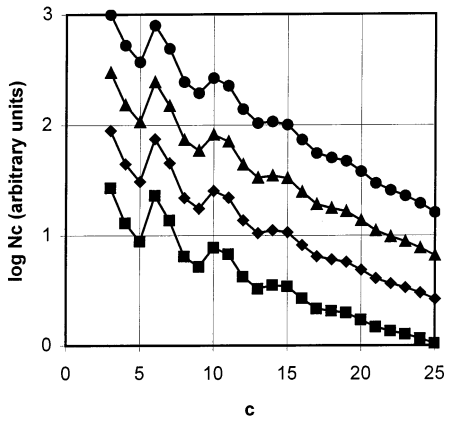

Figure 15. Distribution of volatile (ANE*s* + ENE*s*) (N_c) by carbon number (*c*) from superposition of 50% BB products predicted by the kinetic model and 50% RS products from a statistical distribution at 550 °C: ■, $s = 0.07$ ($m = -0.044$, $v = 0.139$); ♦, $s = 0.09$ ($m = -0.053$, $v = 0.138$); ▲, $s = 0.11$ ($m = -0.062$, $v = 0.138$); ●, $s = 0.13$ ($m = -0.071$, $v = 0.138$). Ordinates offset by arbitrary amounts for clarity.

negative *m* as the RS component by definition shifts to smaller average *c*, but the effect on *v* is negligible.

There is a subtle interplay between the assigned RS:BB ratio and the assignments of k_{1x} used in the model. As seen above, the *v* value for the BB component alone depends strongly on the proportion of 1,5- compared with 1,4- and 1,6-shifts (Figure 12). However, for any given set of k_{1x} assignments and their associated BB profile, the *v* value for the composite can also be modulated by the amount of RS added. For example, consider at 500 °C the case 2 extreme with no k_{1x} selectivity for which the "BB only" *v* value is inherently low (0.10; Figure 12) and not incommensurate with experimental data (Table 2 and Figure 2). However, this same low *v* value could be reproduced with the more selective base rate constants (case 1), for which inherently $v = 0.241$ (Figure 12), by superimposing 69 wt % RS with $s = 0.09$. For the extreme case 3 with the highest k_{15} selectivity, for which inherently $v = 0.71$ (Figure 12), 87 wt % RS could be accommodated before *v* was reduced to 0.10. In principle, these three examples with identical *v* values but different BB:RS ratios could be distinguished by their different *m* values, −0.098, −0.048, and −0.043, respectively, but the demands on data quality would be high.

Model Behavior with the Faravelli−Ranzi Rate Constant Assignments. Table 4 contains the only other complete set of rate constant estimates available, those used in the F−R models[30] and derived from earlier compilations by this group for predicting pyrolysis products of linear and branched alkanes.[213,214] Given the different data sources and assumptions used, no systematic trends between this set and ours are to be expected. The F−R values are systematically larger, except for the k_β values for *sec* radicals, and the incremental differences decrease with increasing *T*, except for the k_β's. Although the individual F−R rate constants for the 1,*x*-shift are larger, the ratio of k_{14}:k_{15}:k_{16} is quite similar, e.g., 6:68:27 for the (p,s) processes for our set vs 8:69:22 for the F−R set at 500 °C, and the inequality $k_{14} < k_{16}$, dampened with increasing *T*, pertains for both sets. Summary model output for the F−R set at 500 °C is given in Table 5. The major differences compared with our predictions are that BB is less competitive compared with RS at all *T*, owing to the smaller F−R assignment for k_β(s,p) which is rate-limiting for effective BB, and that UZ is increased, albeit still minor, at high *T*, owing to the larger F−R assignment for k_β(p,p). The major change in (ANE + ENE) volatiles distribution is a less negative value of *m′*. This larger average distance of the 1,*x*-shift into the chain for the F−R set, especially at higher *T*, follows directly from the lower assigned value of the ratio k_β(s,p)/k_{1x}-(s,s). Correspondingly, *v* decreased somewhat as increased 1,*x*-shift compared with β-scission allows greater opportunity for "equilibration" among P*m*R. The tendency for broadening of the predicted ANE and ENE maxima at higher *c* values toward the next higher *c* is slightly reduced compared with our set, owing to the F−R k_{14}/k_{16} ratio being somewhat nearer unity.

Summary Observations from Model. *Predicted Ratios of Pathways: Absolute Values.* The prediction that UZ should be the least favored process at all *T* values (Figure 10) is clearly supported by the data, and this pathway will not be discussed further. Comparing the predicted product profiles from BB alone (with a trivial contribution from UZ) in Figure 11 with the data in Figures 2 and 3 confirms the conventional wisdom that a mixture of RS and BB is required to reproduce the slopes at high *c* values and the extent of variation between maxima and minima at lower *c* values (*v* is too large from BB alone and too small from RS alone). However, extracting the BB:RS ratio from experimental data on volatile products is not straightforward. The simplest approach has been to take the slope *m* derived from experimental profiles in the higher *c* range as characteristic of the RS component and then equate any positive deviations from the extrapolation to low *c* as definitive of the BB (and UZ) contribution.[217] Yet our model shows that, if modest proportions of 1,4- and 1,6-shift occur along with the dominant 1,5-shift, nontrivial amounts of volatiles are produced by the BB pathway at *every c* value. Thus, the BB component alone has a formal log N_c−*c* profile (e.g., Figures 11 and 12) that could masquerade as a "random" distribution with specific maxima superimposed, albeit with a much more negative slope than typical for RS. For mixed RS and BB, we then expect that the empirical slope *m* from the experimental data will be more negative than the inherent slope for its RS component, and hence the *s*

Table 7. Superpositions of BB/UZ from Model and Statistical RS at 700 °C

line	wt % RS[a]	s_{RS}[b]	m[c]	v[c]
1	0		−0.149	0.286
2	91	0.072	**−0.033**	0.056
3	74	0.069	**−0.033**	0.096
4	62	0.066	**−0.033**	0.118
5	46	0.060	**−0.033**	0.145
6	64	0.072	−0.036	**0.115**
7	64	0.069	−0.034	**0.115**
8	64	0.066	−0.033	**0.115**
9	64	0.060	−0.030	**0.115**

[a] Varied to meet experimental targets of $m = -0.033$ ($s = 0.0732$) or $v = 0.115$ for Ziegler HDPE (ref 58a). [b] Value of s_{RS} assigned for each line. [c] Target value in bold.

value derived from it will be larger than the true s value for the RS component. In summary, this simple deconvolution underestimates the contribution from BB.

To illustrate this conventional and a more complex deconvolution approach, the most consistent data sets appear to be those of the Cantow group[58a] for exhaustive flash pyrolyses at ≤680 °C (Figure 2); we chose the set for Ziegler HDPE for which the parameters are $m = -0.033$ ($c = 16-24$), a derived $s_{exp} = 0.0732$, and $v = 0.115$ ($c = 3-20$).[218] Extrapolating from the $c = 16-24$ region to lower c and equating positive deviations to BB gives BB:RS = ≤17:≥83. For comparison, we apply the alternate approach of superimposing varying amounts of an RS distribution on the BB/UZ distribution from the model until the experimental m and v parameters are matched. The model for BB/UZ alone at 700 °C gives a much more negative $m = -0.149$ and larger $v = 0.286$ (line 1 in Table 7). In lines 2−5, various values of the true s_{RS} for RS, which is necessarily less than $s_{exp} = 0.0732$, were assumed, and the corresponding values of wt % added RS required to force m from −0.149 to the experimental target of −0.033 were calculated. The derived value of v is very sensitive to the assumed value of s_{RS} and the corresponding wt % RS, and the experimental $v = 0.115$ was closely matched near $s = 0.066$ and 62 wt % RS. The inverse procedure was followed in lines 6−9 in which various values of s_{RS} were again assumed, but the corresponding values of wt % added RS required to force v from 0.286 to the experimental target of 0.115 were calculated. The derived value of m is only slightly sensitive to the assumed value of s_{RS}, and minimal variation occurs in the wt % RS required. Hence the v value behaves as the more discriminating descriptor of the experimental data, and a "best match" at ≈700 °C would appear to require BB:RS ≈ 36:64 with $s_{RS} \approx 0.066$ for the RS component.[219] This ratio is indeed larger than that from the simple deconvolution that led to BB:RS = ≤17:≥83. The output from lines 2, 8, and 5 in Table 7 with identical m values but progressively increasing v values of 0.056, 0.115, and 0.145, respectively, is plotted in Figure 16, with the target data ($v = 0.115$) interspersed for comparison. Admittedly judging the quality of match remains somewhat subjective since identical v values do not of course ensure identical product profiles.

Predicted Ratios of Pathways: Effect of Temperature. The predictions from Figure 10 are that RS should dominate at the lowest T and the proportion of BB should increase with increasing T. The significant reductions in MW at the lowest T that precede the evolution of volatiles (Table S1) confirm the first prediction. If the second prediction is correct, the experimental

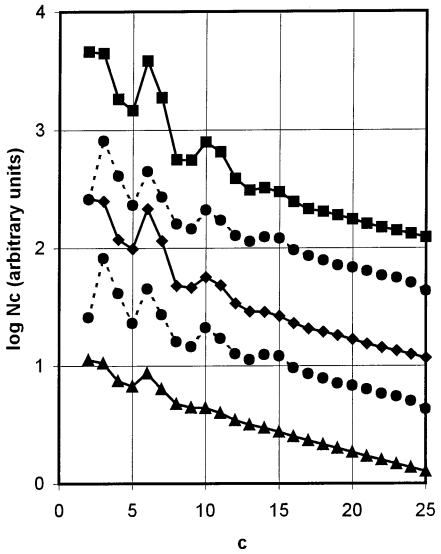

Figure 16. Distribution of volatile (ANEs + ENEs) (N_c) by carbon number (c) from superposition of BB/UZ products predicted by the kinetic model and RS products from a statistical distribution at 700 °C. Solid lines: ■, 46% RS with $s = 0.060$ ($v = 0.145$); ♦, 64% RS with $s = 0.066$ ($v = 0.115$); ▲, 91% RS with $s = 0.072$ ($v = 0.056$); ordinates offset by arbitrary amounts for clarity. Dashed lines: ●, data from exhaustive flash pyrolysis of Ziegler HDPE at ≤680 °C from ref 58a ($v_{exp} = 0.115$); identical plots offset by 1 log unit. All m values have been forced to $m_{exp} = -0.033$ by the BB/UZ:RS ratio used.

v value for the volatiles produced at higher T, indicative of nonstatistical BB products, should increase with increasing T. While the high-T data in Figure 2 appear relatively internally consistent with $v \approx 0.11$, the internally inconsistent low-T data in Figure 3 are too scattered and/or incomplete to test the prediction. Thus, the data of Watanabe and co-workers[75] and Murata and co-workers[19] indeed suggest a notably lower v value, near the RS limit, but the other data[63,64] do not.

Predicted Ratios of Pathways: Effect of Conversion Level. Consideration of the "instantaneous" production of volatiles by BB compared with the "successive" nature of RS (see above) predicts that the apparent BB:RS ratio for the volatiles should decrease as x increases; i.e., v should decrease with increasing x. In addition, since BB produces only ANEs and ENEs while the RS contribution should become progressively richer in DIENES (see above), the ANE:DIENE ratio in the volatiles should decrease with increasing x, with DIENEs concentrated at the higher c values.[220] The paucity of isothermal x-dependent product data available to test these predictions highlights another critical data need. The only modestly diagnostic v* values from the data of De Witt and Broadbelt[64] in closed systems at 420 °C shown in Table 3 do not reveal a trend over the modest x range studied. No major trend is evident either in the data of Ballice and co-workers,[32a] who collected volatile samples as pyrolysis progressed in an open reactor; however, these were T-programmed studies for which any mechanistic trends are further confounded by the T effect on the ease of volatilization.

Predictions Concerning the BB Pathway. The model predicts that the distance of BB into the chain should decrease as T increases (see Figure 11). Results for flash pyrolysis of Ziegler HDPE over the 640−920 °C range[58a] appear to support this trend. The assigned inequality $k_{16} > k_{14}$ leads to the prediction that the local c maxima for ENEs and ANES will be unsymmetrically broadened

toward the next higher *c* value while the reverse inequality predicts the reverse asymmetry. As noted above, there is considerable evidence for the former pattern, e.g., ENE9 < ENE11[30b,63b,67a,72,87] and ANE10 < ANE12,[63b,72b,86a,87] but it is not fully consistent.[64]

Acknowledgment. Research was sponsored by the Division of Chemical Sciences, Geosciences, and Biosciences, Office of Basic Energy Sciences, U.S. Department of Energy, under Contract DE-AC05-00OR22725 with Oak Ridge National Laboratory, managed and operated by UT-Battelle, LLC.

Supporting Information Available: Tables S1−S4 which contain compilations of product data and references; Tables S5−S7 which contain details on selection of Arrhenius parameters for the rate constants used in the model (Table 4); and further textual elaboration on existing mechanistic models for PE pyrolysis, on possible factors that may influence the dependence of k_t on M_n, on possible mechanisms for formation of VL and VD functionality, and on the selection of Arrhenius parameters for the rate constants used in the model (Tables S5−S7). This material is available free of charge via the Internet at http://pubs.acs.org.

References and Notes

(1) (a) Grassie, N.; Scott, G. *Polymer Degradation and Stabilization*; Cambridge University Press: Cambridge, 1985. (b) David, C. In *Comprehensive Chemical Kinetics*; Bamford, C. H., Tipper, C. F. H., Eds.; Elsevier: Amsterdam, 1975; Vol. 14, Chapter 1. (c) Jellinek, H. H. G. In *Aspects of Degradation and Stabilization of Polymers*; Jellinek, H. H. G., Ed.; Elsevier: Amsterdam, 1978; Chapter 1. (d) Mita, I. In *Aspects of Degradation and Stabilization of Polymers*; Jellinek, H. H. G., Ed.; Elsevier: Amsterdam, 1978; Vol. 1, Chapter 6. (e) Stivala, S. S.; Kimura, J.; Reich, L. In *Degradation and Stabilization of Polymers*; Jellinek, H. H. G., Ed.; Elsevier: Amsterdam, 1983; Chapter 1. (f) Mita, I.; Horie, K. In *Degradation and Stabilization of Polymers*; Jellinek, H. H. G., Ed.; Elsevier: Amsterdam, 1983; Chapter 5. (g) Madorsky, S. L. *Thermal Degradation of Organic Polymers*; Interscience: New York, 1964. (h) Blazso, M. *J. Anal. Appl. Pyrolysis* **1997**, *39*, 1. (i) For an earlier partial review for PE, see: Paabo, M.; Levin, B. C. *Fire Mater.* **1987**, *11*, 55.

(2) Kroschwitz, J. I., Ed. *Encyclopedia of Polymer Science and Engineering*, 2nd ed.; Wiley: New York, 1986; Vol. 6, pp 383−521.

(3) HDPE typically has one methyl terminus while the other may be methyl, vinyl, or another group formed by catalyst quenching; it typically has only a few (0.5−3/1000C) short-chain branches (SCB). The unsaturation in Phillips HDPE is largely terminal vinyl (TV; RCH═CH_2) while Ziegler HDPE typically has a mixture of TV, vinylidene (VD; R_2C═CH_2), and *trans*-vinylene groups (VL; RCH═CHR) in a ratio of ≈3:1:1. LDPE contains more SCBs in the range C_2−C_8 (10−30/1000C), which result from a 1,*x*-hydrogen shift during polymerization (ref 5), as well as long-chain branches (LCB) (0.5−4/1000C), which result from transfer during polymerization. It typically has one double bond per molecule but with VD being 5−10 times more prevalent than TV and VL groups.

(4) Early data exist for polymethylene (PM), prepared by Lewis acid-catalyzed polymerization of diazomethane, that is in principle even less branched than HDPE; however, these materials have typically not been well characterized.

(5) (a) Roedel, M. J. *J. Am. Chem. Soc.* **1953**, *75*, 6110. (b) Willbourn, A. H. *J. Polym. Sci.* **1959**, *34*, 569.

(6) (a) Noffz, D.; Pfab, W. *Fresenius Z. Anal. Chem.* **1967**, *228*, 188. (b) Lichtenstein, N.; Quellmalz, K. *Staub Reinhalt. Luft* **1986**, *46*, 11.

(7) (a) Willmott, F. W. *J. Chromatogr. Sci.* **1969**, *7*, 101. (b) Data at 480 °C from ref 7a are not included in Figure 1 because of uncertainty about the conversion factors from area % to mol %.

(8) Sodero, S. F.; Berruti, F.; Behie, L. A. *Chem. Eng. Sci.* **1996**, *51*, 2805.

(9) Seeger, M.; Gritter, R. J. *J. Polym. Chem., Polym. Chem. Ed.* **1977**, *15*, 1393.

(10) Ng, S. H.; Seoud, H.; Stanciulescu, M.; Sugimoto, Y. *Energy Fuels* **1995**, *9*, 735.

(11) Ding, W.; Liang, J.; Anderson, L. L. *Fuel Process. Technol.* **1997**, *51*, 47.

(12) Murty, M. V. S.; Grulke, E. A.; Bhattacharyya, D. *Polym. Degrad. Stab.* **1998**, *61*, 421.

(13) (a) McCaffrey, W. C.; Brues, M. J.; Cooper, D. G.; Kamal, M. R. *J. Appl. Polym. Sci.* **1996**, *60*, 2133. (b) McCaffrey, W. C.; Cooper, D. G.; Kamal, M. R. *Polym. Degrad. Stab.* **1998**, *62*, 513. (c) McCaffrey, W. C.; Cooper, D. G.; Kamal, M. R. *J. Appl. Polym. Sci.* **1999**, *73*, 1415.

(14) Uddin, M. A.; Koizumi, K.; Murata, K.; Sakata, Y. *Polym. Degrad. Stab.* **1997**, *56*, 37.

(15) Park, J. J.; Park, K.; Park, J.-W.; Kim, D. C. *Korean J. Chem. Eng.* **2002**, *19*, 658.

(16) McCaffrey, W. C.; Kamal, M. R.; Cooper, D. G. *Polym. Degrad. Stab.* **1995**, *47*, 133.

(17) (a) Kastner, H.; Kaminsky, W. *Hydrocarbon Proc.* **1995**, 109. (b) Kaminsky, W.; Schlesselmann, B.; Simon, C. *J. Anal. Appl. Pyrolysis* **1995**, *32*, 19. (c) Predel, M.; Kaminsky, W. *Polym. Degrad. Stab.* **2000**, *70*, 373.

(18) (a) Aguado, R.; Olazar, M.; San Jose, M. J.; Gaisan, B.; Bilbao, J. *Energy Fuels* **2002**, *16*, 1429. (b) Aguado, R.; Olazar, M.; Gaisan, B.; Prieto, R.; Bilbao, J. *Ind. Eng. Chem. Res.* **2002**, *41*, 4559.

(19) Murata, K.; Hirano, Y.; Sakata, Y.; Uddin, M. A. *J. Anal. Appl. Pyrolysis* **2002**, *65*, 71.

(20) (a) Conesa, J. A.; Font, R.; Marcilla, A.; Garcia, A. N. *Energy Fuels* **1994**, *8*, 1238. (b) Conesa, J. A.; Font, R.; Marcilla, A. *Energy Fuels* **1997**, *11*, 126. (c) Conesa, J. A.; Font, R.; Marcilla, A.; Caballero, J. A. *J. Anal. Appl. Pyrolysis* **1997**, *40−41*, 419. (d) Conesa, J. A.; Font, R. *Energy Fuels* **1999**, *13*, 678.

(21) (a) Lovett, S.; Berruti, F.; Behie, L. A. *Ind. Eng. Chem. Res.* **1997**, *36*, 4436. (b) Milne, B. J.; Behie, L. A.; Berruti, F. *J. Anal. Appl. Pyrolysis* **1999**, *51*, 157.

(22) Williams, P. T.; Williams, E. A. *J. Anal. Appl. Pyrolysis* **1999**, *51*, 107.

(23) Mastellone, M. L.; Perugini, F.; Ponte, M.; Arena, U. *Polym. Degrad. Stab.* **2002**, *76*, 479.

(24) (a) Mastral, F. J.; Esperanza, E.; Garcia, P.; Juste, M. *J. Anal. Appl. Pyrolysis* **2002**, *63*, 1. (b) Berrueco, C.; Mastral, F. J.; Esperanza, E.; Ceamanos, J. *Energy Fuels* **2002**, *16*, 1148. (c) Mastral, F. J.; Esperanza, E.; Berrueco, C.; Juste, M.; Ceamanos, J. *J. Anal. Appl. Pyrolysis* **2003**, *70*, 1.

(25) (a) Westerhout, R. W. J.; Waanders, J.; Kuipers, J. A. M.; van Swaaij, W. P. M. *Ind. Eng. Chem. Res.* **1998**, *37*, 2293. (b) Westerhout, R. W. J.; Waanders, J.; Kuipers, J. A. M.; van Swaaij, W. P. M. *Ind. Eng. Chem. Res.* **1998**, *37*, 2316. (c) Westerhout, R. W. J.; Kuipers, J. A. M.; van Swaaij, W. P. M. *Ind. Eng. Chem. Res.* **1998**, *37*, 841. (d) Westerhout, R. W. J.; Waanders, J.; Kuipers, J. A. M.; van Swaaij, W. P. M. *Ind. Eng. Chem. Res.* **1997**, *36*, 1955.

(26) Cozzani, V.; Nicolella, C.; Rovatti, M.; Tognotti, L. *Ind. Eng. Chem. Res.* **1997**, *36*, 342. (b) Font, R. Aracil, I.; Fullana, A.; Martin-Gullon, I.; Conesa, J. A. *J. Anal. Appl. Pyrolysis* **2003**, *68−69*, 599.

(27) Much of the ethylene and propylene appears to be formed by further RS of larger initial fragments in a consecutive, but mechanistically analogous, fashion. We prefer to characterize this free-radical RS continuum by "early-late" nomenclature and limit the more common term "secondary reactions" to those that obviously involve additional mechanisms, such as the formation of aromatics.

(28) Dickens, B. *J. Polym. Sci., Polym. Chem. Ed.* **1982**, *20*, 1065.

(29) Ceamanos, J.; Mastral, J. F.; Millera, A.; Aldea, M. E. *J. Anal. Appl. Pyrolysis* **2002**, *65*, 93.

(30) (a) Ranzi, E.; Dente, M.; Faravelli, T.; Bozzano, G.; Fabini, S.; Nava, R.; Cozzani, V.; Tognotti, L. *J. Anal. Appl. Pyrolysis* **1997**, *40−41*, 305. (b) Faravelli, T.; Bozzano, G.; Scassa, C.; Perego, M.; Fabini, S.; Ranzi, E.; Dente, M. *J. Anal. Appl. Pyrolysis* **1999**, *52*, 87. Cf.: Faravelli, T.; Bozzano, G.; Colombo, M.; Ranzi, E.; Dente, M. *J. Anal. Appl. Pyrolysis*, in press.

(31) (a) Sezgi, N. A.; Cha, W. S.; Smith, J. M.; McCoy, B. J. *Ind. Eng. Chem. Res.* **1998**, *37*, 2582. (b) Kodera, Y.; McCoy, B. J. *Energy Fuels* **2002**, *16*, 119.

(32) (a) Ballice, L.; Yuksel, M.; Saglam, M.; Reimert, R.; Schulz, H. *Energy Fuels* **1998**, *12*, 925. (b) Ballice, L. *Fuel* **2001**, *80*, 1923.

(33) (a) Bockhorn, H.; Hornung, A.; Hornung, U.; Schawaller, D. *J. Anal. Appl. Pyrolysis* **1999**, *48*, 93. (b) Bockhorn, H.; Hornung, A.; Hornung, U. *J. Anal. Appl. Pyrolysis* **1999**, *50*,

77. (c) Bockhorn, H.; Hentschel, J.; Hornung, A.; Hornung, U. *Chem. Eng. Sci.* **1999**, *54*, 3043.
(34) (a) Peterson, J. D.; Vyazovkin, S.; Wight, C. A. *Macromol. Chem. Phys.* **2001**, *202*, 775. (b) Gao, Z.; Amasaki, I.; Kaneko, T.; Nakada, M. *Polym. Degrad. Stab.* **2003**, *81*, 125.
(35) (a) Staggs, J. E. J. *Polym. Degrad. Stab.* **2002**, *76*, 37. (b) Gao, Z.; Amasaki, I.; Nakada, M. *J. Anal. Appl. Pyrolysis* **2003**, *67*, 1. (c) Conesa, J. A.; Caballero, J. A.; Reyes-Labarta, J. A. *J. Anal. Appl. Pyrolysis*, in press.
(36) Simha, R.; Wall, L. A. *J. Polym. Sci.* **1951**, *6*, 39.
(37) Conesa, J. A.; Marcilla, A.; Font, R.; Caballero, J. A. *J. Anal. Appl. Pyrolysis* **1996**, *36*, 1.
(38) Note that this "kinetic order" n applies to the weight of sample remaining in a system of constantly decreasing volume, not to the usual concentration of reactant in a constant volume system. The "concentration" of key reactive groups in the residue does not directly track increasing x; e.g., the concentration of reactive C−H bonds in degrading PE will be essentially constant, but that of unsaturated groups will increase. Cf.: Grimbley, M. R.; Lehrle, R. S. *Polym. Degrad. Stab.* **1995**, *48*, 441. Bate, D. M.; Lehrle, R. S.; Pattenden, C. S.; Place, E. J. *Polym. Degrad. Stab.* **1998**, *62*, 73.
(39) Bockhorn, H.; Hornung, A.; Hornung, U.; Jakobstroer, P. *J. Anal. Appl. Pyrolysis* **1999**, *49*, 53.
(40) (a) Kodera, Y.; McCoy, B. J. *AIChE J.* **1997**, *43*, 3205. (b) Wang, M.; Smith, J. M.; McCoy, B. J. *AIChE J.* **1995**, *41*, 1521. (c) McCoy, B. J.; Madras, G. *AIChE J.* **1997**, *43*, 802. (d) Madras, G.; McCoy, B. J. *Catal. Today* **1998**, *40*, 321. (e) Kruse, T. M.; Woo, O. S.; Broadbelt, L. J. *Chem. Eng. Sci.* **2001**, *56*, 971. (f) Smagala, T. G.; McCoy, B. J. *Ind. Eng. Chem. Res.* **2003**, *42*, 2461.
(41) (a) For a recent ambitious example for polystyrene of combining the method of moments with thermochemical kinetic estimates of rate constants for elementary steps. Kruse, T. M.; Woo, O. S.; Wong, H.-W.; Khan, S. S.; Broadbelt, L. J. *Macromolecules* **2002**, *35*, 7830. Kruse, T. M.; Wong, H.-W.; Broadbelt, L. J. *Ind. Eng. Chem. Res.* **2003**, *42*, 2722. (b) Minimal kinetic data at higher T, for which TGA techniques are no longer applicable, is available from filament pyrolyzers. Aguado and co-workers (ref 18b) recently compared rates of volatilization at 500−600 °C in a filament pyrolyzer and a conical spouted-fluidized-bed reactor. The formal first-order rate constants for both HDPE and LDPE were ≈20-fold greater in the latter configuration, suggestive that the filament pyrolyzer with small samples still may suffer from mass transfer restrictions to volatilization or uncertainties in T.
(42) Oakes, W. G.; Richards, R. B. *J. Chem. Soc.* **1949**, 2929.
(43) Wall, L. A.; Madorsky, S. L.; Brown, D. W.; Straus, S.; Simha, R. *J. Am. Chem. Soc.* **1954**, *76*, 3430.
(44) Arnett, R. L.; Stacy, C. J. *Polym. Eng. Sci.* **1966**, *6*, 295.
(45) Quackenbos, H. M. *Polym. Eng. Sci.* **1966**, *6*, 117.
(46) (a) Holmstrom, A.; Sorvik, E. *J. Chromatogr.* **1970**, *53*, 95. (b) Holmstrom, A.; Sorvik, E. M. *J. Appl. Polym. Sci.* **1974**, *18*, 761.
(47) (a) Kuroki, T.; Sawaguchi, T.; Niikuni, S.; Ikemura, T. *Macromolecules* **1982**, *15*, 1460. (b) Kuroki, T.; Sawaguchi, T.; Niikuni, S.; Ikemura, T. *J. Polym. Sci., Polym. Chem. Ed.* **1983**, *21*, 703.
(48) Rangarajan, P.; Bhattacharyya, D.; Grulke, E. *J. Appl. Polym. Sci.* **1998**, *70*, 1239.
(49) Guy, L.; Fixari, B. *Polymer* **1999**, *40*, 2845.
(50) Moriya, T.; Enomoto, H. *Polym. Degrad. Stab.* **1999**, *65*, 373.
(51) van Grieken, R.; Serrano, D. P.; Aguado, J.; Garcia, R.; Rojo, C. *J. Anal. Appl. Pyrolysis* **2001**, *58*−*59*, 127.
(52) Ekenstam, A. *Chem. Ber.* **1936**, *69*, 553.
(53) Kumar, G. S.; Kumar, V. R.; Madras, G. *J. Appl. Polym. Sci.* **2002**, *84*, 68.
(54) Witt, D. R.; Hogan, J. P. *J. Polym. Sci., Part A-1* **1970**, *8*, 2689.
(55) Tanaka, K.; Takakura, M.; Koshino, Y. *J. Appl. Polym. Sci.* **1974**, *18*, 1131.
(56) Bailey, W. J.; Liotta, C. L. *Prepr. (Am. Chem. Soc., Div. Polym. Chem.)* **1964**, *5*, 333.
(57) (a) van Schooten, J.; Evenhuis, J. K. *Polymer* **1965**, *6*, 343. (b) van Schooten, J.; Evenhuis, J. K. *Polymer* **1965**, *6*, 561.
(58) (a) Michajlov, L.; Zugenmaier, P.; Cantow, H.-J. *Polymer* **1968**, *9*, 325. (b) Michajlov, L.; Cantow, H.-J.; Zugenmaier, P. *Polymer* **1971**, *12*, 70.
(59) Liebman, S. A.; Ahlstrom, D. H.; Starnes, W. H., Jr.; Schilling, F. C. *J. Macromol. Sci., Chem.* **1982**, *A17*, 935.
(60) Haney, M. A.; Johnston, D. W.; Clampitt, B. H. *Macromolecules* **1983**, *16*, 1775.
(61) Gorecki, T.; Poerschmann, J. *Anal. Chem.* **2001**, *73*, 2012.
(62) Madorsky, S. L.; Straus, S.; Thompson, D.; Williamson, L. *J. Polym. Sci.* **1949**, *4*, 639.
(63) (a) Tsuchiya, Y.; Sumi, K. *J. Polym. Sci., Polym. Chem. Ed.* **1968**, *6*, 415. (b) Tsuchiya, Y.; Sumi, K. *J. Polym. Sci., Part B: Polym. Lett.* **1968**, *6*, 357.
(64) De Witt, M. J.; Broadbelt, L. J. *Energy Fuels* **2000**, *14*, 448.
(65) Jalil, P. A. *J. Anal. Appl. Pyrolysis* **2002**, *65*, 185.
(66) (a) GC data qualitatively similar to those in Table S2 have been presented for LDPE pyrolyzed at 350 °C for 2 h in an evacuated sealed tube (ref 66b) and for HDPE pyrolyzed in a reactive distillation apparatus with slow heatup to 440 °C (ref 13c). In contrast, a recent claim (ref 31a) that pyrolysis of a very low-MW HDPE at 370−410 °C for 1−3 h gave only ANEs in the C_{1-5} fraction is atypical. (b) Mordi, R. C.; Fields, R.; Dwyer, J. *J. Anal. Appl. Pyrolysis* **1994**, *29*, 45.
(67) (a) Wampler, T. P.; Levy, E. J. *Analyst* **1986**, *111*, 1065. (b) Wampler, T. P. *J. Anal. Appl. Pyrolysis* **1989**, *15*, 187.
(68) Dolezal, Z.; Pacakova, V.; Kovarova, J. *J. Anal. Appl. Pyrolysis* **2001**, *57*, 177.
(69) Some uncertainty relates to the data in ref 68 because C_1 and C_2 were reported together.
(70) Chiu, J. *Anal. Chem.* **1968**, *40*, 1516.
(71) Iida, T. A.; Honda, K.; Nozaki, H. *Bull. Chem. Soc. Jpn.* **1973**, *46*, 1480.
(72) (a) Kiran, E.; Gillham, J. K. *J. Appl. Polym. Sci.* **1976**, *20*, 931. (b) Kiran, E.; Gillham, J. K. *J. Appl. Polym. Sci.* **1976**, *20*, 2045.
(73) Ohkita, H.; Nishiyama, R.; Tochihara, Y.; Mizushima, T.; Kakuta, N.; Morioka, Y.; Ueno, A.; Namiki, Y.; Tanifuji, S.; Katoh, H.; Sunazuka, H.; Nakayama, R.; Kuroyanagi, T. *Ind. Eng. Chem. Res.* **1993**, *32*, 3112.
(74) Blazso, M.; Zelei, B.; Jakab, E. *J. Anal. Appl. Pyrolysis* **1995**, *35*, 221.
(75) Watanabe, M.; Hirakoso, H.; Sawamoto, S.; Adschiri, T.; Arai, K. *J. Supercrit. Fluids* **1998**, *13*, 247.
(76) Lehrle, R. S.; Rollinson, M.; Dadvand, N.; Parsons, I. W. *Polym. Degrad. Stab.* **1999**, *66*, 221.
(77) Use of cyclohexane as extraction solvent precluded analysis for C_{6-7}, values for C_5 were felt by the authors to be experimentally low, and values for C_{25-34} (ANEs and ENEs not resolved) were also felt to be low because of incomplete extraction. The reported x is a minimum because it was defined in terms of GC-detectable products rather than total weight loss.
(78) Lattimer, R. P. *J. Anal. Appl. Pyrolysis* **1995**, *31*, 203.
(79) Beckey, H. D. *Principles of Field Ionization and Field Desorption Mass Spectrometry*; Pergamon Press: Oxford, 1977. Beckey notes that sensitivity factors for ANEs and ENEs have quite different dependences on c for low c, but that these may be less pronounced for higher c.
(80) A similar disparity between GC and FIMS data would result if the loss of transfer efficiency for higher-c products in GC runs were highly selective for condensation/sorption of ENEs compared with ANEs.
(81) Schulten, H.-R.; Simmleit, N.; Muller, R. *Anal. Chem.* **1987**, *59*, 2903.
(82) Watanabe, C.; Kawahara, Y.; Ohtani, H.; Tsuge, S. *J. Anal. Appl. Pyrolysis* **2002**, *64*, 197.
(83) Wall, L. A.; Flynn, J. H.; Straus, S. *J. Phys. Chem.* **1970**, *74*, 3237.
(84) Kudchadker, A. P.; Zwolinski, B. J. *J. Chem. Eng. Data* **1966**, *11*, 253.
(85) (a) Cieplinski, E. W.; Ettre, L. S.; Kolb, B.; Kemmner, G. *Fresenius Z. Anal. Chem.* **1964**, *205*, 357. (b) Kolb, B.; Kemmner, G.; Kaiser, K. H.; Cieplinski, E. W.; Ettre, L. S. *Fresenius Z. Anal. Chem.* **1965**, *209*, 302.
(86) (a) Seeger, M.; Cantow, H.-J. *Makromol. Chem.* **1975**, *176*, 1411. (b) Seeger, M.; Cantow, H.-J. *Polym. Bull. (Berlin)* **1979**, *1*, 347.
(87) Sugimura, Y.; Tsuge, S. *Macromolecules* **1979**, *12*, 512.
(88) Staudinger, H.; Steinhofer, A. *Justus Liebigs Ann. Chem.* **1935**, *517*, 35.
(89) Burk, R. E. *J. Phys. Chem.* **1931**, *35*, 2446.
(90) (a) Simha, R.; Wall, L. A.; Blatz, P. J. *J. Polym. Sci.* **1950**, *5*, 615. (b) Simha, R.; Wall, L. A. *J. Phys. Chem.* **1952**, *56*, 707.
(91) (a) Rice, F. O. *J. Am. Chem. Soc.* **1931**, *53*, 1959. (b) Rice, F. O.; Herzfeld, K. F. *J. Am. Chem. Soc.* **1934**, *56*, 284. (c) Kossiakoff, A.; Rice, F. O. *J. Am. Chem. Soc.* **1943**, *65*, 590. (d) Fabuss, B. M.; Smith, J. O.; Satterfield, C. N. *Adv. Petr. Chem. Refining* **1964**, *9*, 157.

(92) For substituted vinyl polymers, $(CH_2CRX)_n$, additional steps involving positional isomeric radicals are of course involved.

(93) In step 1b, "Y" is some irregularity such as an allylic C−C bond adjacent to unsaturation, a branch point, a head-to-head rather than head-to-tail sequence, trace peroxides incorporated during radical polymerization, or terminal initiator residues.

(94) Koenig, T.; Fischer, H. In *Free Radicals*; Kochi, J. K., Ed.; Wiley-Interscience: New York, 1973; Vol. I, Chapter 4.

(95) de Gennes, P.-G. *Scaling Concepts in Polymer Physics*; Cornell University Press: Ithaca, NY, 1979. de Gennes, P. G. *J. Chem. Phys.* **1971**, *55*, 572.

(96) Doi, M.; Edwards, S. F. *The Theory of Polymer Dynamics*; Clarendon Press: Oxford, 1986.

(97) Jellinek (ref 1c) asserted, somewhat improbably, that "radicals succeed only rarely in diffusing out of the cage to make scissions permanent.... It is fortunate that there is such a great tendency in polymers to mend broken main chain links before these breaks become permanent, otherwise stable polymers would scarcely exist."

(98) The hypothesis of exclusive nonchain in-cage operation of steps 1, 6a, and 6b (ref 44) and the accompanying suggestion that transfer is not important in "static" systems but may become so in "flowing" systems contain the unlikely implicit assumption that macroscopic mixing can disrupt a molecular-level cage.

(99) Note that $R_s^\bullet$ almost surely also undergoes 1,x-shifts and transfer, but these do not achieve chemical change although they serve to equilibrate the positional isomers and MWD of $R_s^\bullet$.

(100) For small radicals, k_{comb}/k_{dispr} is larger for *prim* than for *sec* radicals and also probably decreases with increasing *T*. Gibian, M. J.; Corley, R. C. *Chem. Rev.* **1973**, *73*, 441.

(101) Inversely, the mere presence of monomer in the volatiles does not diagnose UZ because it can also be formed in step 4d.

(102) Wall, L. A.; Florin, R. E. *J. Res. Natl. Bur. Stand.* **1958**, *60*, 451.

(103) (a) Benson, S. W. *Thermochemical Kinetics*; Wiley-Interscience: New York, 1976. (b) Benson, S. W. *The Foundations of Chemical Kinetics*; McGraw-Hill: New York, 1960.

(104) (a) Poutsma, M. L. *Energy Fuels* **1990**, *4*, 113. (b) Poutsma, M. L. *J. Anal. Appl. Pyrolysis* **2000**, *54*, 5.

(105) A further simplifying assumption was that $R_p^\bullet$ and allyl radical were kinetically equivalent.

(106) This group asserted that "according to the long chain-reaction approximation, [initiation] reactions, although necessary to complete the mechanism, have a negligible effect on the overall rate of the reaction" rather than the correct statement that they "...make negligible contribution to the stoichiometric consumption of polymer." Hence in their attempts to deconvolute E_{exp} values, they ignored the often arithmetically dominant "$^1/_2E_i$" term (ref 40a).

(107) Mita's estimate of ≈1−10 for polystyrene is also in qualitative agreement with experiment. For polymers with quaternary carbons that totally unzip (very large $\bar{\epsilon}$), he postulated that k_β is enhanced by steric repulsions among successive chain substituents that would not accumulate in small-molecule models. An alternate proposal[1a,c] is that the UZ pathway predominates in these cases by default because transfer is retarded by the absence of reactive *tert* on-chain hydrogens (of course both "effects" may reinforce each other); this rationalization would not correctly predict the minimal UZ of PE which has no *tert* hydrogens. Mita considered only β-scission of the substituted chain-end $\sim CH_2CRX^\bullet$ radical. In fact, β-scission of the less stabilized nonsubstituted $\sim CRXCH_2^\bullet$, which has typically been ignored in the literature, must also be considered since it will be formed in equivalent amounts in step 1 and exclusively by step 3b for quaternary-center polymers.

(108) To illustrate the data inconsistencies in the literature, Ceamanos and co-workers (ref 29) obtained $A_{exp} = 2.5 \times 10^{15}$ s^{-1} and $E_{exp} = 59.5$ kcal mol^{-1} but constant *n* over a similar *T* range.

(109) Note that if termination in fact occurred largely through $R_s^\bullet$ rather than $R_p^\bullet$, the form of the analogously derived volatilization rate would depend on the relative magnitudes of k_{4a} and $k_{3a}[P]$. If $k_{4a} \gg k_{3a}[P]$, the $C[P]^{0.5} + C'[P]^{1.5}$ form would persist; if instead $k_{4a} \ll k_{3a}[P]$, the form would be $C[P]^{-0.5} + C'[P]^{0.5}$.

(110) The corresponding values for LDPE were similar: $A = 2 \times 10^{-2}$ (6.7×10^{-3}) s^{-1} and $E = 8.5$ (28.4) kcal mol^{-1}.

(111) Dente, M.; Bozzano, G.; Bussani, G. *Comput. Chem. Eng.* **1997**, *21*, 1125.

(112) Stein, S. E.; Robaugh, D. A.; Alfieri, A. D.; Miller, R. E. *J. Am. Chem. Soc.* **1982**, *104*, 6567. Stein, S. E. *J. Am. Chem. Soc.* **1981**, *103*, 5685. Poutsma, M. L. *Fuel* **1980**, *59*, 335.

(113) Whereas the authors assumed termination through $R_p^\bullet$, the inequality $k_\beta \ll k_H(\rho/m_0)$ suggests that $R_s^\bullet$ would be the more prevalent radical for termination (see text).

(114) While they used backbone rather than TV end-group allylic homolysis as the initiating event, they included specific (but not quantitatively stated) rate constant enhancement factors both for abstraction of allylic hydrogens and for β-scission steps that generated allylic radicals.

(115) BB was included by introducing a parameter α_i, the fraction of any given radical that undergoes a 1,*i*-shift rather than β-scission. This alters the stoichiometric balance equations and adds additional terms to the formation−consumption equations for each X_n species. For example, $ANE_n \rightarrow ENE_j + ANE_{n-j}$ becomes $ANE_n \rightarrow ENE_j + (1 - \sum_i\alpha_i)ANE_{n-j} + 0.5\sum_i\alpha_i[(ANE_{n-j-(i+1)} + ENE_{i+1}) + (ENE_{n-j-(i-2)} + ANE_{i-2})]$.

(116) Sawaguchi, T.; Saito, H.; Yano, S.; Seno, M. *Polym. Degrad. Stab.* **2001**, *72*, 383. Sawaguchi, T.; Ikemura, T.; Seno, M. *Macromolecules* **1995**, *28*, 7973.

(117) Sawaguchi, T.; Seno, M. *Polymer* **1996**, *37*, 3697. Sawaguchi, T.; Ikemura, T.; Seno, M. *Polymer* **1996**, *37*, 5411. Sawaguchi, T.; Seno, M. *Polymer* **1996**, *37*, 5607. Sawaguchi, T.; Seno, M. *Polym. Degrad. Stab.* **1996**, *54*, 33. Kuroki, T.; Sawaguchi, T.; Suzuki, K.; Ide, S.; Ikemura, T. *Polymer* **1983**, *24*, 428.

(118) (a) When these pyrolyses were repeated to the same final *T* values but with much slower heating rates of 5−60 °C/min rather than 20 °C/ms, the ANE:DIENE ratios increased with decreasing heating rate. While the authors (ref 67a) suggested that slower heating rates may reveal more of the "primary ANE" products that are formed at lower *T* and swept out before "secondary DIENE" products can be formed at higher *T*, a simpler rationalization would be that, as the heating rate is decreased, the bulk of the degradation occurs at a progressively lower average *T*, for which the ANE:DIENE ratio is inherently higher, as suggested by the flash pyrolysis results. (b) Pacakova, V.; Nogatz, M.; Novak, V. *Collect. Czech. Chem. Commun.* **1982**, *47*, 509.

(119) Jellinek, H. H. G. *Trans. Faraday Soc.* **1944**, *40*, 266. Jellinek, H. H. G. *Trans. Faraday Soc.* **1948**, *44*, 345.

(120) (a) Stull, D. R.; Westrum, E. F., Jr.; Sinke, G. C. *The Chemical Thermodynamics of Organic Compounds*; Wiley: New York, 1969. (b) Blanksby, S. J.; Ellison, G. B. *Acc. Chem. Res.* **2003**, *36*, 255. (c) Cohen, N. *J. Phys. Chem.* **1992**, *96*, 9052; cf.: Janoschek, R.; Rossi, M. J. *Int. J. Chem. Kinet.* **2002**, *34*, 550. (d) Kerr, J. A.; Stocker, D. W. In *CRC Handbook of Chemistry and Physics*, 83rd ed.; CRC Press: Boca Raton, FL, 2002.

(121) (a) Tsang, W. *J. Phys. Chem. Ref. Data* **1988**, *17*, 887. (b) Tsang, W. *J. Phys. Chem. Ref. Data* **1990**, *19*, 1. (c) Tsang, W. *J. Phys. Chem. Ref. Data* **1991**, *20*, 221. (d) Tsang, W.; Hampson, R. F. *J. Phys. Chem. Ref. Data* **1986**, *15*, 1087. (e) *NIST Standard Reference Database 17, Version 7.0 (Web Version)*, 2000.

(122) (a) Lias, S. G.; Liebman, J. F.; Levin, R. D.; Kafifi, S. A.; Stein, S. E. *NIST Standard Reference Data Base 25; Structures and Properties; Ver 2.02*, 1994. Group contributions to $\Delta H_f^\circ{}_{298}$ values for radicals embedded in the NIST program were slightly adjusted to conform to more recent generic $D°$(C−H) values as described in ref 122b. (b) Poutsma, M. L. *Energy Fuels* **2002**, *16*, 964.

(123) Ruchardt, C.; Gerst, M.; Ebenhoch, J. *Angew. Chem., Int. Ed. Engl.* **1997**, *36*, 1406.

(124) Even if we were to accept the questionable (ref 112) reduction in E_{homo} of 5.3 kcal mol^{-1} proposed (ref 111) to accompany the transposition from the gaseous to condensed state for the butane model, a major disparity in favor a long KCL would still remain.

(125) (a) Further indirect evidence for long KCL at least for allylic end-group homolysis is the only modest selectivity to propylene which should be the ultimate transfer product from allyl radical (refs 47a, 56, and 63a). Willmott (ref 7a) did suggest a correlation between the modest amount of propylene formed and the extent of terminal unsaturation in the starting PE. (b) Bailey and Liotta (ref 56) suggested that a nonradical concerted retroene reaction at TV groups should also be considered as a source of propylene. However, were this process to be significantly more rapid than the overall radical chain processes, much more propylene would

be expected since the retroene process could then "unzip" an entire vinyl-terminated chain.
(126) (a) Buback, M.; Egorov, M.; Gilbert, R. G.; Kaminsky, V.; Olaj, O. F.; Russell, G. T.; Vana, P.; Zifferer, G. *Macromol. Chem. Phys.* **2002**, *203*, 2570. (b) Mita, I.; Horie, K. *J. Macromol. Sci., Rev. Macromol. Chem. Phys.* **1987**, *C27*, 91.
(127) (a) Kremer, K.; Grest, G. S.; Carmesin, I. *Phys. Rev. Lett.* **1988**, *61*, 566. (b) Kreer, T.; Baschnagel, J.; Muller, M.; Binder, K. *Macromolecules* **2001**, *34*, 1117. (c) van Ruymbeke, E.; Keunings, R.; Tanaka, M.; Iwata, K.; Kuzuu, N. *Comput. Theor. Polym. Sci.* **2000**, *10*, 299. (d) Stephenne, V.; Hagenaars, A.; Bailly, C. *Macromolecules* **2002**, *35*, 2689. (e) Harmandaris, V. A.; Mavrantzas, V. G.; Theodorou, D. N.; Kroger, M.; Ramirez, J.; Ottinger, H. C.; Vlassopoulos, D. *Macromolecules* **2003**, *36*, 1376.
(128) Rouse, P. E. Jr. *J. Chem. Phys.* **1953**, *21*, 1271.
(129) (a) Welp, K. A.; Wool, R. P.; Agrawal, G.; Satija, S. K.; Pispas, S.; Mays, J. *Macromolecules* **1999**, *32*, 5127. (b) Putz, M.; Kremer, K.; Grest, G. S. *Europhys. Lett.* **2000**, *52*, 721.
(130) Lin, Y.-H.; Juang, J.-H. *Macromolecules* **1999**, *32*, 181.
(131) Refinements of the classic reptation theory continue to be made (refs 127b, 127c, and 132), and there remains considerable discussion concerning the exact definition of "entanglement," the optimal specification of N_e, and its derivation from various experimental variables (refs 129b, 130, and 133).
(132) Des Cloizeaux, J. *Europhys. Lett.* **1988**, *5*, 437. Hua, C. C. *J. Chem. Phys.* **2000**, *112*, 8176 and references therein. Semenov, A. N.; Rubinstein, M. *Eur. Phys. J. B* **1998**, *1*, 87.
(133) For recent examples, see: (a) Putz, M.; Kremer, K.; Grest, G. S. *Europhys. Lett.* **2000**, *49*, 735. (b) Wischnewski, A.; Richter, D. *Europhys. Lett.* **2000**, *52*, 719. (c) Szamel, G.; Wang, T. *J. Chem. Phys.* **1997**, *107*, 10793. (d) Fetters, L. J.; Lohse, D. J.; Richter, D.; Witten, T. A.; Zirkel, A. *Macromolecules* **1994**, *27*, 4639. (e) Kavassalis, T. A.; Noolandi, J. *Macromolecules* **1989**, *22*, 2709. (f) Schieber, J. D. *J. Chem. Phys.* **2003**, *118*, 5162.
(134) Lin, Y.-H. *Macromolecules* **1987**, *20*, 3080.
(135) O'Shaughnessy, B.; Yu, J. *Macromolecules* **1998**, *31*, 5240 and references therein.
(136) de Gennes, P. G. *J. Chem. Phys.* **1982**, *76*, 3316, 3326.
(137) Lodge, T. P. *Phys. Rev. Lett.* **1999**, *83*, 3218.
(138) Friedman, B.; O'Shaughnessy, B. *Macromolecules* **1993**, *26*, 5726.
(139) (a) Wall, L. A.; Florin, R. E. *J. Res. Natl. Bur. Stand.* **1958**, *60*, 451. (b) Flynn, J. H.; Wall, L. A. *J. Polym. Sci., Polym. Lett. Ed.* **1967**, *5*, 191.
(140) Yang, J.; Miranda, R.; Roy, C. *Polym. Degrad. Stab.* **2001**, *73*, 455.
(141) Madorsky, S. L. *J. Res. Natl. Bur. Stand.* **1959**, *62*, 219.
(142) Simha, R.; Wall, L. A. *J. Phys. Chem.* **1952**, *56*, 707.
(143) Wall, L. A.; Straus, S. *J. Polym. Sci.* **1960**, *44*, 313.
(144) Madorsky, S. L. *J. Polym. Sci.* **1952**, *9*, 133.
(145) Kuhn, W. *Chem. Ber.* **1930**, *63*, 1503.
(146) Lehrle, R.; Williams, R.; French, C.; Hammond, T. *Macromolecules* **1995**, *28*, 4408.
(147) Emsley, A. M.; Heywood, R. J. *Polym. Degrad. Stab.* **1995**, *49*, 145.
(148) Since various approaches lead to different formulations for the proportionality constant, we focus on the $(1 - s)^{(c-1)}$ term that is common to all.
(149) This idealized statistical result is unlikely to be fully rigorous for small c values for which specific mechanistic anomalies associated with end groups would become non-negligible.
(150) In contrast to the "smooth" curves in Figure 2 for the range $c \approx 12-25$, plots (not shown) of data from Faravelli and co-workers (ref 30b), limited to the ENEs from HDPE at 600 °C ($x = 1$) and 500 °C ($x < 1$), show significant minima centered at $c = 17$, which were not predicted by their model (see text). The ANE:ENE:DIENE patterns described in Table S4 do not suggest any unusual maxima in ANEs or DIENEs to counteract these atypical minima.
(151) Numerical integration was performed with the Acuchem Series 4.0 programs with the "integration tolerance" set at the suggested value of 0.001. Braun, W.; Herron, J. T.; Kahaner, D. K. *Int. J. Chem. Kinet.* **1988**, *20*, 51.
(152) All time units and concentrations are relative for assumed first-order behavior; all derived values of s are also only of relative, not absolute, significance for this scaling exercise.
(153) Mole and weight fraction calculations assume that the molecular mass of P(n) scales as n.
(154) The wt % of products with $n \leq 9$ formed from the P(19) actually converted has a lower limit of 26.3% ($\sum_1^9 n/\sum_1^{18} n$).
(155) For P(19), $t_{1/2} = (\ln 2)/18 = 0.0385$.
(156) This scaling result is qualitatively the same as that portrayed in Figure 2 of ref 35a.
(157) (a) Kreglewski, A.; Zwolinski, B. J. *J. Phys. Chem.* **1961**, *65*, 1050. (b) Kudchadker, A. P.; Zwolinski, B. J. *J. Chem. Eng. Data* **1966**, *11*, 253.
(158) Using instead a geometric progression between P(9) and P(1), i.e., $\log k_{evap} \propto -n$, led to qualitatively identical trends in simulation output.
(159) From pyrolysis−FIMS results (see above), Lattimer (ref 78) proposed BB with a very large number of serial shifts required before β-scission; e.g., the maximum near $c = 36$ would require 8−9 shifts.
(160) Wall, L. A. *J. Res. Natl. Bur. Stand.* **1948**, *41*, 315.
(161) Bailey and Liotta (ref 56) reported an atypically large increase in selectivity to ethylene among the C_{2-5} gases when T was increased from 415 to 600 °C and suggested that it was largely a primary ("early") product because it did not increase further as t at 600 °C was increased from 1 to10 min; however, the pyrolysis was likely already complete after the 1 min run.
(162) (a) Domine, F. *Energy Fuels* **1989**, *3*, 89. (b) Wu, G.; Katsumura, Y.; Matsuura, C.; Ishigure, K. *Ind. Eng. Chem. Res.* **1996**, *35*, 4747. (c) Jackson, K. J.; Burnham, A. K.; Braun, R. L.; Knauss, K. G. *Org. Geochem.* **1995**, *23*, 941. (d) Khorasheh, F.; Gray, M. R. *Ind. Eng. Chem. Res.* **1993**, *32*, 1853. (e) Ford, T. J. *Ind. Eng. Chem. Fundam.* **1986**, *25*, 240.
(163) Fischer, H.; Radom, L. *Angew. Chem., Int. Ed.* **2001**, *40*, 1340.
(164) While modest selectivity in hydrogen abstraction to form $R_t^\bullet$ compared with $R_s^\bullet$ is reasonable, a source of selectivity for attack adjacent to a branch site is not obvious.
(165) Only 2-propyl, 2-butyl, and 3-pentyl are inaccessible for $x = 4-6$.
(166) Expressions given in three-parameter Arrhenius format to accommodate curved Arrhenius plots over large T ranges were converted to two-parameter format at a median pyrolysis T of 773 K; the error introduced for k values then calculated at, say, 673 or 873 K, is trivial compared with the likely absolute errors.
(167) We have slightly adjusted the value for $k_{H,773}$(s,p) to improve internal consistency. For the p,s ⇄ s,p interconversion, the recommended rate constants give $K_{773} = (2 \cdot 3.4)/(6 \cdot 0.47) = 2.4$ compared with 4.1 based on the estimated thermochemical parameters ($\Delta H^o_{773} = -2.9$ kcal mol^{-1} and $\Delta S^o_{773} = -0.9$ cal mol^{-1} K^{-1}) (ref 122a). Compare the selectivity pattern down the first column (1.0:3.4:8.4) with that across the first row (1.0:2.1^{-1}:10.4^{-1}). If $k_{H,773}$(s,p)^{rel} were decreased from 0.47 to 0.29 = 3.4^{-1}, these patterns would be more self-consistent and K_{773} would become 3.9, in perfect accord with thermochemical balance. Therefore we made this small adjustment, arbitrarily divided between log A and E.
(168) Camaioni, D. M.; Autrey, S. T.; Salinas, T. B.; Franz, J. A. *J. Am. Chem. Soc.* **1996**, *118*, 2013. Ma, X.; Schobert, H. H. *Prepr. (Am. Chem. Soc., Div. Fuel Chem.)* **2001**, *46* (2), 369. Ma, X.; Schobert, H. H. *Ind. Eng. Chem. Res.* **2003**, *42*, 1151.
(169) (a) Bencsura, A.; Knyazev, V. D.; Xing, S.-B.; Slagle, I. R.; Gutman, D. *Symp. Int. Combust. Proc.* **1992**, *24*, 629. (b) Knyazev, V. D.; Slagle, I. R. *J. Phys. Chem.* **1996**, *100*, 5318. (c) Slagle, I. R.; Batt, L.; Gmurczyk, G. W.; Gutman, D. *J. Phys. Chem.* **1991**, *95*, 7732. (d) Knyazev, V. D.; Dubinsky, I. A.; Slagle, I. R.; Gutman, D. *J. Phys. Chem.* **1994**, *98*, 11099.
(170) The analogous values for isobutyl, $k_\beta = 2(10^{14.19}) \exp(-31850/RT)$ s^{-1} (ref 169b), and neopentyl, $3(10^{13.42}) \exp(-30900/RT)$ s^{-1} (ref 169c), lead to $k_{\beta,773}$(p,Me)^{rel} values per methyl group of 1:8:3, somewhat sensitive to the substitution pattern at the α-carbon but not in a monotonic trend.
(171) Gang, J.; Pilling, M. J.; Robertson, S. H. *J. Chem. Soc., Faraday Trans.* **1997**, *93*, 1481.
(172) Yamauchi, N.; Miyoshi, A.; Kosaka, K.; Koshi, M.; Matsui, H. *J. Phys. Chem. A* **1999**, *103*, 2723.
(173) Imbert and Marshall (ref 174) deduced k_β(s,p) = $10^{13.3} \exp(-30000/RT)$ s^{-1} for 2-hexyl and hence a 2.4-fold lower value of $k_{\beta,773}$(s,p)^{rel} while Baldwin and co-workers (ref 175) deduced a single-T value for $k_{\beta,753}$(s,p) for 2-pentyl, which is 2.5-fold larger than predicted by the Yamauchi expression (ref 172).

(174) Imbert, F. E.; Marshall, R. M. *Int. J. Chem. Kinet.* **1987**, *19*, 81.
(175) Baldwin, R. R.; Bennett, J. P.; Walker, R. W. *J. Chem. Soc., Faraday Trans. 1* **1980**, *76*, 1075.
(176) Poutsma, M. L.; Schaffer, S. R. *J. Phys. Chem.* **1973**, *77*, 158.
(177) Watkins, K. W. *Can. J. Chem.* **1972**, *50*, 3738.
(178) Marshall, R. M. *Int. J. Chem. Kinet.* **1990**, *22*, 935. Tsang, W.; Walker, J. A.; Manion, J. A. *Proc. 27th Int. Symp. Combust.* **1998**, *1*, 135.
(179) We note a modest discrepancy with an *estimated* value of $k_{14}(s,s) = 2(10^{10.20}) \exp(-17000/RT)$ for 2-octyl → 4-octyl at much lower T (385 K) (ref 180), which would correspond to a 4.5-fold larger value if extrapolated to 773 K.
(180) Dobe, S.; Berces, T.; Reti, F.; Marta, F. *Int. J. Chem. Kinet.* **1987**, *19*, 895.
(181) Note that this recommendation for $k_{15}(p,s)$ includes a tunneling correction while that for $k_{14}(p,s)$ does not.
(182) Watkins, K. W. *J. Phys. Chem.* **1973**, *77*, 2938.
(183) A recent ab initio calculation for 1-hexyl (ref 184) gave an A value $10^{1.1}$-fold higher; that for 1-heptyl was $10^{1.3}$-fold higher still; calculations of E at the level of theory used were not considered chemically reliable.
(184) Toh, J. S.-S.; Huang, D. M.; Lovell, P. A.; Gilbert, R. G. *Polymer* **2001**, *42*, 1915.
(185) Smith, M. B.; March, J. *March's Advanced Organic Chemistry. Reactions, Mechanisms, and Structure*, 5th ed.; Wiley-Interscience: New York, 2001.
(186) Lehrle, R. S.; Pattenden, C. S. *Polym. Degrad. Stab.* **1999**, *63*, 153.
(187) Larson, C. W.; Chua, P. T.; Rabinovitch, B. S. *J. Phys. Chem.* **1972**, *76*, 2507.
(188) (a) Randall, J. C. *J. Macromol. Sci., Rev. Macromol. Chem. Phys.* **1989**, *C29*, 201. (b) Hay, J. N.; Mills, P. J.; Ognjanovic, R. *Polymer* **1986**, *27*, 677. (c) Usami, T.; Takayama, S. *Macromolecules* **1984**, *17*, 1756. (d) Mattice, W. L.; Stehling, F. C. *Macromolecules* **1981**, *14*, 1479. (e) Axelson, D. E.; Levy, G. C.; Mandelkern, L. *Macromolecules* **1979**, *12*, 41. (f) Bovey, F. A.; Schilling, F. C.; McCrackin, F. L.; Wagner, H. L. *Macromolecules* **1976**, *9*, 76.
(189) Ohtani, H.; Tsuge, S.; Usami, T. *Macromolecules* **1984**, *17*, 2557.
(190) Interestingly, the probabilities increased again for $x = 9-14$ to small but nonnegligible values. This approach also suggested that an alkyl branch on the chain modestly promotes the achievement of the cyclic transition state.
(191) Viskolcz, B.; Lendvay, G.; Seres, L. *J. Phys. Chem. A* **1997**, *101*, 7119. Viskolcz, B.; Lendvay, G.; Kortvelyesi, T.; Seres, L. *J. Am. Chem. Soc.* **1996**, *118*, 3006.
(192) All the models and calculations noted conclude that 1,3-shift is of trivial importance because of the major increase in strain associated with a four-membered ring. The ethyl SCBs in PE are generally ascribed to an indirect mechanism (ref 5b) not involving a 1,3-shift, although this is not universally accepted (ref 60).
(193) We have chosen not to include shifts for $x > 6$, although the SCB evidence may indicate $k_{17} \geq k_{14}$.
(194) Zoller, P.; Walsh, D. J. *Standard Pressure−Volume−Temperature Data for Polymers*; Technomic Publishing Co.: Lancaster, PA, 1995.
(195) Capt, L.; Kamal, M. R. *Int. Polym. Process.* **2000**, *15*, 83.
(196) (a) Much earlier data in a small range just above the melting point gave $(1/\rho) = 1.152 + 8.8 \times 10^{-4}T$ (ref 197); extrapolation of this correlation leads to p values that are ≈0.06 units higher near 750 °C. (b) Chiang, R.; Flory, P. J. *J. Am. Chem. Soc.* **1961**, *83*, 2857. Gubler, M. G.; Kovacs, A. J. *J. Polym. Sci.* **1959**, *34*, 551. Quinn, F. A., Jr.; Mandelkern, L. *J. Am. Chem. Soc.* **1958**, *80*, 3178.
(197) Measurements in the range 151−295 °C were fit to $\rho = 0.999 - 1.6 \times 10^{-3}T + 2 \times 10^{-6}T^2$ (ref 31a). However, this expression does not reproduce the results plotted in the paper and would lead to increasing p with increasing T if extrapolated above 400 °C.
(198) Flory, P. J. *Principles of Polymer Chemistry;* Cornell University Press: Ithaca, NY, 1953; Chapter 3.
(199) Winnik, M. A.; Maharaj, U. *Macromolecules* **1979**, *12*, 902.
(200) Evidence for diminished reactivity of polystyrene and polypropylene in solution toward the *tert*-butoxy radical, a moderately chemically activated example, compared with small-molecule models remains surprising. The authors of this study (ref 201) considered a true "polymer effect" in which hydrogens in the interior of a polymer coil were shielded from the attacking radical; such an "effect" is again not likely relevant to a melt.
(201) Niki, E.; Kamiya, Y. *J. Org. Chem.* **1973**, *38*, 1403. Niki, E.; Kamiya, Y. *J. Chem. Soc., Perkin Trans. 2* **1975**, 1221.
(202) Watanabe, M.; Tsukagoshi, M.; Hirakoso, H.; Adschiri, T.; Arai, K. *AIChE J.* **2000**, *46*, 843.
(203) For example, both the first and second propagation rate constants for methyl acrylate (MA) were determined to be at least 10-fold greater than k_p (ref 204a); the first propagation rate constants for methyl methacrylate (MMA) and methacrylonitrile (MAN) were determined to be 17-fold and 6-fold greater, respectively, than k_p (ref 204b), and similar differences have been claimed for styrene (ref 204c).
(204) (a) Moad, G.; Rizzardo, G.; Solomon, D. H.; Beckwith, A. L. J. *Polym. Bull. (Berlin)* **1992**, *29*, 647. (b) Gridnev, A. A.; Ittel, S. D. *Macromolecules* **1996**, *29*, 5864. (c) Morrison, B. R.; Casey, B. S.; Lacik, I.; Leslie, G. L.; Sangster, D. F.; Gilbert, R. G.; Napper, D. H. *J. Polym. Sci., Polym. Chem. Ed.* **1994**, *32*, 631. Deady, M.; Mau, A. W. H.; Moad, G.; Spurling, T. H. *Makromol. Chem.* **1993**, *194*, 1691. Olaj, O. F.; Vana, P.; Zoder, M. *Macromolecules* **2002**, *35*, 1208. Zetterlund, P. B.; Busfield, W. K.; Jenkins, I. D. *Macromolecules* **2002**, *35*, 7232.
(205) If the P*n*R involved in forming PENE*n* happened to be a near-end P*m*R (formed either by direct transfer from P, 1,*x*-shift within P*n*R, or further transfer between P*n*R and P), there would be an added contribution from the resulting ∑ENE*r* and ∑PENE*m* that is not included in this definition. However, for large MW and hence $m \ll n$, this correction is trivial and any ENEs so formed would be statistically distributed without any of the specificity characteristic of BB.
(206) Although only a single value of $k_\beta(s,p)$ is used in the model, β-scission toward the chain interior slightly exceeds that toward the chain end (ratio ≈ 1.07) because the latter process is not available to P2R and limited for P3R by a smaller value of $k_\beta(s,Me)$.
(207) 1,*x*-Shifts and β-scissions in both directions are included in this generic ratio, although some of these processes may not be structurally allowed for small m.
(208) The chosen lower limit of $c = 3$ purposely excludes the ENE2Z formed from UZ, and the chosen upper limit of $c = 20$ minimizes perturbations caused by the truncation of the P*m*R series at $m = 30$.
(209) The changes were apportioned equally between log A (±0.5 log units) and E (±1.77 kcal mol^{-1}) at 500 °C, and hence the differences will be slightly larger/smaller at lower/higher T.
(210) The simulations for the largest k_{1x} values were characterized by a major increase in the amount of truncation as the population of P*m*R with $m > 30$ became for the first time nontrivial.
(211) Simulations with k_{14} and k_{16} set to zero of course gave even sharper maxima. However, minor amounts of volatiles were still formed at other than the "magic" c values; these are derived from successive formation of Ar1R, Ar6R, ... and β-scission of the latter.
(212) Because of the truncation at $c = 25$, the actual "wt % RS" will be somewhat larger because the RS contribution extends further toward higher c values than does the BB contribution. For the most conservative assumption that *no* BB products occur for $c > 25$ (the simulation begins to become statistically unreliable at this point because of the truncation at $m = 30$), the actual wt % RS values over the c range to 1−100 (the RS contribution becomes vanishingly small for $c > 100$) would be 32.6, 64.3, and 77.1 wt % rather than 25, 50, and 75 wt %.
(213) Ranzi, E.; Faravelli, T.; Gaffuri, P.; Sogaro, A. *Combust. Flame* **1995**, *102*, 179. Ranzi, E.; Dente, M.; Pierucci, S.; Biardi, G. *Ind. Eng. Chem. Fundam.* **1983**, *22*, 132.
(214) Numerous other sources for rate constant assignments are available (ref 215), including several used to model the pyrolysis of hexadecane (refs 162d, 202, and 216), but none provide a complete set.
(215) Allara, D. L.; Shaw, R. *J. Phys. Chem. Ref. Data* **1980**, *9*, 523. Nigam, A.; Klein, M. T. *Ind. Eng. Chem. Res.* **1993**, *32*, 1297. De Witt, M. J.; Dooling, D. J.; Broadbelt, L. J. *Ind. Eng. Chem. Res.* **2000**, *39*, 2228. Bounaceur, R.; Warth, V.; Marquaire, P.-M.; Scacchi, G.; Domine, F.; Dessort, D.; Pradier, B.; Brevart, O. *J. Anal. Appl. Pyrolysis* **2002**, *64*, 103.
(216) Doue, F.; Guiochon, G. *J. Chim. Phys. Physiochim. Biol.* **1968**, *65*, 395. Doue, F.; Guiochon, G. *Can. J. Chem.* **1969**,

47, 3477. Depeyre, D.; Flicoteaux, C. *Ind. Eng. Chem. Res.* **1991**, *30*, 1116. Khorasheh, F.; Gray, M. R. *Ind. Eng. Chem. Res.* **1993**, *32*, 1853. Ristori, A.; Dagaut, P.; Cathonnet, M. *Combust. Flame* **2001**, *125*, 1128. Watanabe, M.; Adschiri, T.; Arai, K. *Ind. Eng. Chem. Res.* **2001**, *40*, 2027.

(217) For a detailed illustration of this approach applied to polyisobutylene, see: Lehrle, R. S.; Pattenden, C. S. *Polym. Degrad. Stab.* **1999**, *63*, 321.

(218) The parameters of $m = -0.037$, $s_{exp} = 0.082$, and $v = 0.110$ for Phillips HDPE are not likely statistically different, given our derivation of the values from reading graphical data from the original publication.

(219) This treatment assumes of course that our assignments of k_{1x} ($x = 4-6$) are correct. We have seen in Table 6 the strong dependence of the inherent v for the BB component on these assignments. Hence, any evaluation of the BB:RS ratio is also dependent on the k_{1x} ratios. For example, repeating the exercise in Table 7 for case 3 in Table 6, that with the highest selectivity for 1,5-shift, would give the best match at of course a higher proportion of unselective RS, specifically 84 wt % RS with $s \approx 0.072$.

(220) As a possible example of the latter phenomenon for polypropylene, see ref 78.

MA0303768